ALMA MATER STUDIORUM
UNIVERSITÀ DI BOLOGNA

DEPARTMENT OF INDUSTRIAL CHEMISTRY "TOSO MONTANARI"

SECOND CYCLE DEGREE IN

LOW CARBON TECHNOLOGIES AND SUSTAINABLE CHEMISTRY

CLASSE LM-71 - SCIENZE E TECNOLOGIE DELLA CHIMICA INDUSTRIALE

Solid State NMR of Tin-based Perovskites

Supervisor
Prof. Daniele Cortecchia

Candidate
Michela Cecconi

Co-Supervisors
Prof. Cristina Femoni
Doctor Giulia Martelli

October 2024

Academic Year 2023/2024

Abstract

Metal halide perovskites (MHPs) have attracted significant attention in the last decades due to their exceptional optoelectronic properties, particularly in the fields of photovoltaic panels and light-emitting devices. While most progress has been made with lead (Pb)-based perovskites due to their excellent solar cell performance, it is widely known that lead is toxic and environmentally harmful. As a result, tin (Sn(II)) based perovskites, have emerged as a promising alternative. However the poor stability of tin and its tendency to oxidize have hindered the development of these materials. The slow pace of progress in this field is also due to a scarcity of methods capable of probing the microstructure and supramolecular environment of perovskites, which is essential for improving their stability and performance. This work seeks to characterize two tin based perovskites, $FASnI_3$ (3D) and PEA_2SnI_4 (2D), by solid-state NMR and single-crystal X-ray diffraction (SCXRD), with the purpose of granting a comprehensive understanding of their structure and dynamics. In fact, solid state NMR can provide an in-depth analysis of the local environments of individual atoms, as well as their orientation and mobility, while XRD offers a broader view of their 3D crystalline structure. The focus is primarily on PEA_2SnI_4, as it was observed that the use of two distinct precursors, SnO and SnI_2, generated significant differences in both ss-NMR spectra and XRD data, suggesting that the choice of precursor affects the material's structure and order. This study highlights the potential of solid-state NMR in advancing research on tin-based perovskites and it opens the door for future exploration of how structural disorder impacts their performance.

Contents

Introduction: Perovskites

Perovskites are crystalline structures named after the naturally occurring mineral Perovskite, or calcium titanate, with chemical formula $CaTiO_3$. Nowadays the name Perovskite is applied to the class of materials that shares the same crystal structure as the original mineral, described by the formula: ABX_3. In this representation, the B-site is occupied by metals with a small ionic radius in the form of divalent cations, which can be part of the transition metal series, such as lead (Pb) and tin (Sn). The B site cations have a 6-fold coordination with the X site anions. This arrangement leads to the formation of a cubic unit cell, where each B-site cation is surrounded by 6 X-site anions in an octahedral coordination. The X site is commonly occupied by either oxygen (O^{2-}), or halide anions (X^-), which will respectively form perovskite oxides and halide perovskites. Finally, A is a small organic or inorganic cation which should fit inside the cubo-octahedral cavities between the cubic cells formed by B and X. Organic cations are generally larger than inorganic ones, but the perovskite structure is wide enough to accommodate small organic cations in the cavities, allowing for organic-inorganic hybridization. Perovskites are one of the most abundant and versatile structural families, capable of forming a vast array of compounds. This allows for the formation of numerous types of perovskites, each with distinct crystalline structures. In fact, depending on the type of cation that occupies the A site, perovskites can form 3D or 2D compounds. At the same time, there is the possibility to form mixed perovskites, which involve the partial substitution of the ions of either site, leading to compositions like $(A_1A_2)BX_3$ or $AB(X_1X_2)_3$. Ultimately, as mentioned before, when the X site is occupied by a halide anion, Metal Halide Perovskites (MHPs) are formed, which have gained particular interest during the years due to their outstanding optical and electronic properties, which will be discussed further in the following paragraphs, as this work is focused on the development and improvement of this

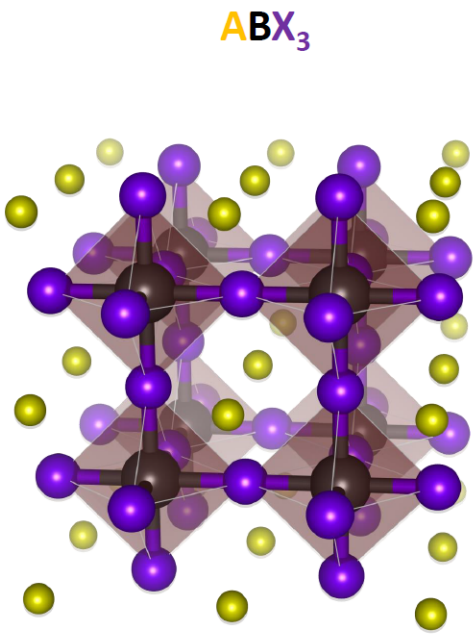

Figure 1.1: Representation of a cubic perovskite unit cell

incredible class of compounds.[1]

1.1 Metal Halide Perovskites

Metal halide perovskites exhibit unique electronic and crystalline structures that endows them with excellent optoelectronic properties, including a tunable band gap, high defect tolerance, and high absorption coefficients. Moreover, they exhibit high structural tunability because of the variety of ions that can be incorporated in the structure. Nonetheless their production process remains relatively cheap. Their potential as remarkably efficient solar cell absorbers was first demonstrated in the beginning of the 2010s. Specifically, the most known and developed class of MHPs is given by lead (Pb) based perovskites, which exhibit a power conversion efficiency (PCE) of over 22%. Their general formula is $APbX_3$. As stated in the previous paragraph, the A site cation of Metal Halide perovskites can be occupied by organic or inorganic cations that differ depending on the spacial dimension of the perovskite. There are 3 main A-site cations that can be used for designing 3D MHPs: Methylammonium (MA = $CH_3NH_3^+$); Formamidinium (FA = $HC(NH_2)_2^+$) and Cesium (Cs^{+2}). This is due to shape and size by which these cations are characterized, that allows them to fit into the interstitial spaces present in the inorganic lattice of the perovskite. This spacial restrictions are the reason why only a few cations are actually suited for 3D

MHPs formation. In fact, if the size of the A site cation becomes larger than the cavities, layered 2D perovskites are formed. The A-site molecules that can be incorporated by lower dimensional perovskites are typically ammonium-containing large cations with long alkyl chains or aromatic rings, where the most commonly used is Phenethylammonium ($C_6H_5CH_2CH_2NH_3^+$ or PEA) [1]. Because of this characteristic structure, 2D MHPs are generally less hygroscopic compared to their 3D counterparts, but at the same time, their charge-carrier transport properties can be inferior to those of 3D perovskite materials [2]. The characteristics of both 2D and 3D perovskites and therefore the causes behind these variations will be discussed further in the next paragraphs.

1.1.1 MHP crystalline structure

As previously mentioned, MHPs can present different dimensionalities, (from 3D to 0D). For the aim of this work, only 3D and 2D structures will be discussed.

3D MHPs

3D MHPs have an ideal cubic structure, where the centre is occupied by the B cation and each vertex is given by $[BX_6]^{-4}$. The bond lengths and angles of the crystalline structure are determined by the size of each ion, which are often described by the Goldschmith tolerance factor. In fact depending on the choice of ions, the ideal structure can be shifted by a certain degree. The Goldshchmidt factor τ is a ratio of ionic radii and it is used to determine the distortion of crystal structures in terms of the constituent ionic packing and therefore their geometric stability. It is given by the equation:

$$\tau = \frac{R_a + R_x}{\sqrt{2}(R_b + R_x)} \tag{1.1}$$

Where the relative dimensions of the perovskite cations (R_a, R_b, R_x) determine the actual possibility of formation of the perovskite from a purely geometric point of view. In an ideal cubic structure where $0.9 < \tau < 1$ the A, B, and X ions fit almost perfectly into the crystal lattice and the structure is generally stable, but slight distortions may occur, which generally remain insignificant. While if $0.8 < \tau < 0.9$, further deviations could cause more serious distortions, forcing the structure to adopt lower symmetries, such as orthorhombic. This is due to the lower dimensions of the A-site cations, which cause a

more pronounced octahedral tilting. When $\tau < 0.8$, the 3D perovskite structure is often unstable, because the A-site cation is too small compared to the other two ions. This leads to the collapse of the perovskite structure into a non-perovskitic phase. Finally, if $\tau > 1.1$, 3D perovskites cannot be formed due the large dimensions of the A site cation, that will destabilise the structure. This leads to the formation of the lower dimensional phases, like 1D, 2D and quasi-2D, which bring great interest in nowadays research.

Among 3D MHPs, one of the most studied perovskites are the ones obtained from the FA cation. The crystalline structure of $FASnI_3$, is very similar if not identical to the one of $MASnI_3$, which adopts a cubic unit cell. However, Formamidinium perovskites present a higher degree of structural disorder, which can result in an additional difficulty when analysing the organic phase of this perovskite [3]. Nowadays, more research is being focused on this compound, with the aim of mixing FA with other organic and inorganic cations in order to enhance its properties.

2D MHPs

As previously mentioned, 2D perovskites are formed as a consequence of the insertion in the perovskite lattice, of organic cations that are too large to form 2D perovskites, here these organic spacers can be seen as "scissors" that allow the formation of layered perovskites instead of more compact structures. In fact, typical 2D MHPs are formed by layered sheets, which can be a single atom thick, or a multiple of that [4].

There are two main types of structure that 2D perovskites can form: The Ruddlesden-Popper (RP) and the Dion-Jacobson (DJ), which are depicted in Fig.1.2. The RP general

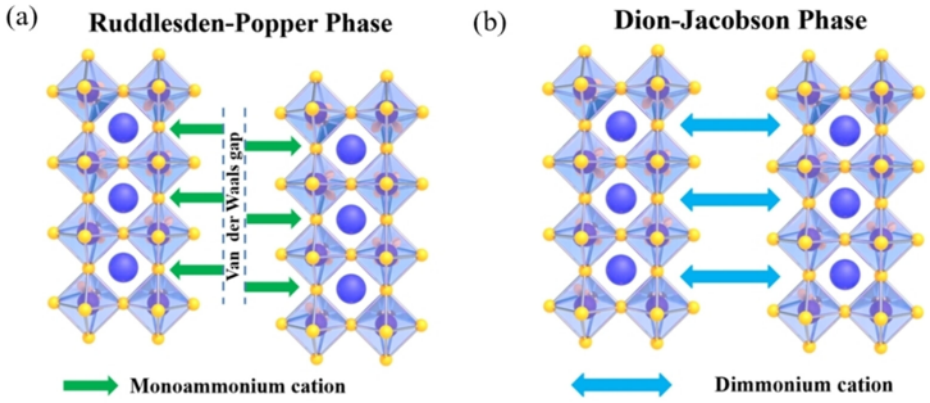

Figure 1.2: Representation of Ruddlesden-Popper(a) and Dion-Jacobson (b) perovskite structures [5].

formula is given by $L_2A_{n-1}B_nX_{3n+1}$, where L is a monovalent hydrophobic organic cation that acts as a protective layer and n is the number of inorganic layers separated by the organic cations. The RP phase is characterised by the presence of two layers of monovalent bulky organic cations (usually ammonium-containing cations [NH_3^+]) that separate the inorganic layers. The organic cations are bonded with the inorganic groups thanks to the formation of hydrogen bonds between the BX_6^{-4} anions and the aminic groups. While the connection between the organic cations of two different layers are given by Van der Waals forces. On the other hand, DJ structures are defined by a single divalent cation that form a bridge between the inorganic layers. They present the following formula: $HA_{n-1}B_nX_{3n+1}$, where H is a bivalent organic interlayer cation. Here the connections between the inorganic layers are stronger because of the presence of a single cation, which makes the structure tighter and more rigid compared to RP [5].

In general, the crystalline structure of MHPs exhibits a tolerance to defects which is better compared to classic semi-conductors. In fact, MHPs performances are not significantly hindered by defects. Since their soft ionic lattice is able to accommodate point defects such as vacancies and interstitial substitutions without drastically affecting the electronic properties [6]. Regardless, defect control and passivation remain essential for achieving successful perovskite preparation. Specifically, since the composition of these perovskites is not limited to the size of the site-A cation, as it is for the 3D ones, the introduction of hydrophobic bulky organic spacers into the perovskite lattice can effectively enhance their stability and performance. Overall, the development of 2D perovskites presents great advantages, primarily because dimensional reduction enables the expansion the perovskite family by providing a vast range of compositional possibilities and customizable features. Additionally, it introduces remarkable structural complexity, enabling precise manipulation of the material's optoelectronic properties.[6]

1.1.2 Electronic properties of MHPs

In order to gain a full picture of the potential of perovskite materials, it is key to understand their electronic properties and how they can be exploited for optoelectronic applications. First and foremost, perovskites are part of the semi conductors family, hence they exhibit a distinct electronic band structure characterized by a *conduction band* (CB) and a *valence band* (VB), with the energy difference between these bands forming the

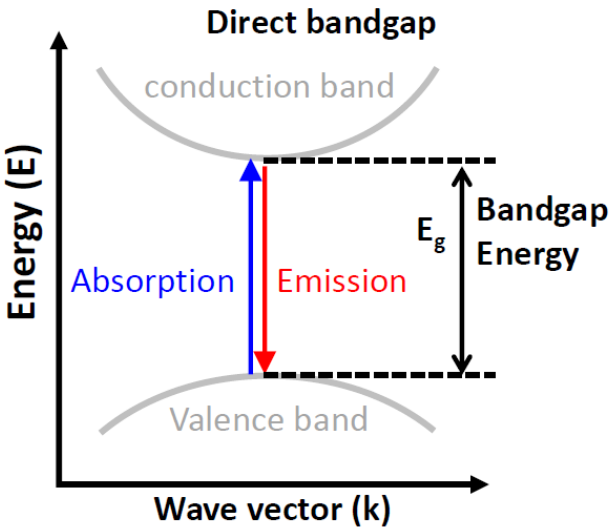

Figure 1.3: Depiction of a semi conductor bandgap and its absorption and emission phenomena [7].

material's bandgap, whose allowed values lie in between the ones of isolating materials and conductors. This confers perovskite materials the fundamental properties needed for the application to technologies such as photovoltaic solar panels and LEDs, since their electrons can be easily excited by the application of a relatively small amount of potential, or by a raise of temperature. In fact, when the material is provided with an energy being equal or greater than the band gap value $Eg = h\nu$, e.g. when a photon is adsorbed, the excited electrons will move to the conduction band, leaving a positive hole behind that can be quickly filled by the next electron, as depicted in Fig.1.3. In an ideal pure semiconductor, this primary electronic excitation will form a free electron-hole pair. If the pair is easily separated, the particles can be called *free carriers*. These particles are typical of crystalline solids with well defined periodicity and space order [7]. When the electron and its associated hole are attracted to each other via Coulomb forces, they can form a quasi-particle called *exciton*. They can be of two main types: Frenkel vs. Wannier excitons. The Wannier excitons are also called *large-radius excitons* or *free excitons* and they are the ones occurring in semi-comductors. The free exciton is overall electrically neutral, contrarily to the Frenkel exciton, therefore it does not transfer charge to the material, but excitation energy [8]. The presence of excitons in perovskites, makes them part of the *intrinsic semiconductors* family [9]. To further explain the optoelectronic characteristics that make MHPs such interesting materials, it can be helpful to have a clear picture of the composition of their electronic structures. In MHPs, the conduction band

is primarily composed of the antibonding interaction between the B-site metal cation's *s*-orbitals and the halide *p*-orbitals, while the valence band is largely derived from the halide *p*-orbitals, as outlined in Fig.1.4. In perovskites, the electronic structure is dominated by the characteristics of the B–X bond, and there is no contribution from the A-site cation. The hybridized nature of the band structure allows MHPs to have tunable bandgaps, typically ranging from 1.5 to 2.3 eV, depending on the choice of halide and B-site cation. All of these characteristics are inherent to perovskite structures in general,

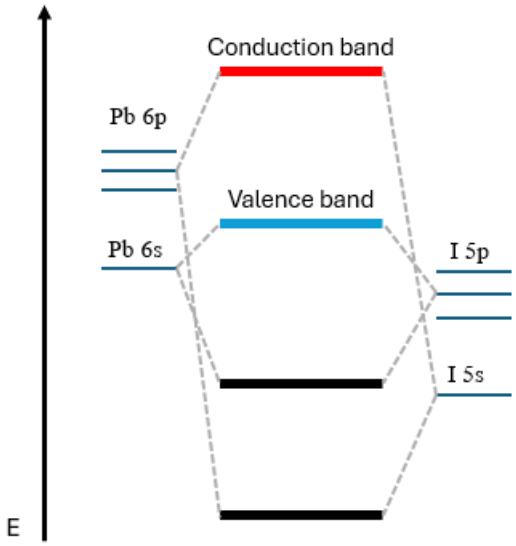

Figure 1.4: Schematic representation of the band gap composition of $MAPbI_3$ [10].

but when talking about 2D perovskites, an additional level of complexity is introduced to the electronic structure, as they form natural multi-quantum well (MQW) systems. These structures are given by the sequentially aligned molecular orbitals of the organic and inorganic layers. In fact, the highest occupied molecular orbital (*HOMO*) and the lowest unoccupied molecular orbital (*LUMO*) of the organic layers are positioned, respectively, below the valence band, and above the conduction band of the inorganic layers. This way, the perovskite inorganic layers will work as quantum wells, enabling the entrance of electronic particles, while the organic spacers serve as barriers, which hinder the path of the electron's movements. This structure, depicted in Fig.1.5 is specifically called *type-I quantum well configuration*, and it allows the confinement of both electrons and holes, which provides an enhancement of the radiative recombination. This can be seen as an advantage to light-emitting applications, while it is not useful, or even disadvantageous

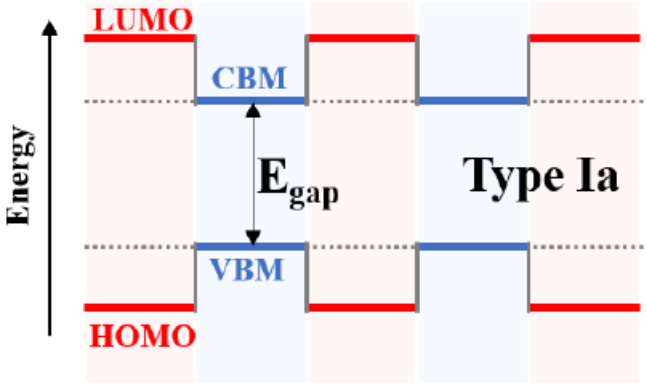

Figure 1.5: Description of a Type 1a quantum well configuration

for solar cells applications [11].

1.1.3 Tin-based perovskites

The most developed family of perovskites until now, has been Lead Halide Perovskites (LHP), and although they have brought an incredible shift to the photovoltaic and optoelectronic fields, LHPs have also presented them with many challenges. Two of the most relevant issues concerns their overall toxicity and low environmental stability, due to the use of Pb [12]. Nowadays, climate change is a serious issue that needs to be tackled with every tool available, and for this reason, the use of lead should be severely decreased or even eliminated. Hence, research is now focused on finding alternatives to lead that wouldn't hinder the properties of perovskites, although the problem is that there are only a few valid options to substitute lead as a B-site cation in perovkites. Among them, the most promising ones are germanium (Ge^{2+}) and tin (Sn^{2+}), which belong to the same group as lead. However, due to its electronic configuration, Ge^{2+} is prone to lose its lone pair electrons, which belong to the s-orbital, leading to poor chemical stability. Therefore, the most favorable alternative remains tin. The Sn^{2+} cation demonstrates excellent optical and electronic properties, which can be even superior to lead-based ones, such as strong optical absorption, and good charge carrier mobility.

The electronic configuration of tin-based perovskites is quite similar to the one presented by LHPs, and their bangap lies between 1.3 and 1.4 eV, which is close to the ideal 1.4 bandgap, but most importantly, Sn-based perovskites' degradation products (SnO ans SnI_4) are much less toxic than their lead-based counterparts [13]. Tin-based perovskites, demponstrate to be very promising for applications on solar cells and optoelectronic de-

vices, as in theory, tin-based solar cells could reach up to 33% PCE, although this limit is still far from being reached, with a current maximum being of 14.81 % [14]. This mainly due to their poor stability when exposed to air, since Sn^{2+} has a tendency to oxidate to Sn^{4+}, which does not form a perovskitic phase. Another important challenge to be faced is the fast crystallization process of these perovskites, that will lead to the formation of in-homogeneous thin films, which present high defect density and low reproducibility rational. This leads to non ideal device performances of tin based perovskites. To tackle this and other issues, various modifications to the compositions and structures of perovskites have been suggested over the years. This is often achieved by incorporating additional ions into the perovskite precursor solution during the preparation process.

Phenethylammonium Tin Iodide

As previously mentioned, one of the most used cations for 2D perovskites is phenethylammonium or PEA, which generates an RP layered perovskites, inserting itself between the inorganic structures of the material. In this paragraph, the properties and characteristics of PEA_2SnI_4 will be briefly discussed. The overall struture of penethylammonium tin iodide perovskite shares the same structure as its lead counterpart, this serves as a strong indicator of the potential electronic properties of this perovskite. When characterised by XRD, the crystal presents directional disorders in both the organic layers and the equatorial iodines, as is depicted in Fig1.6. Nevertheless, this is a common occurrence in layered perovskites, and it should not bring negative effects to the perovskite's applications [14]. The electronic structure of PEA perovskites is classified as type 1a quantum wells, resulting in improved dielectric confinement and high exciton binding energies. While this characteristic can be advantageous for light emission applications, it may also hinder charge carrier extraction in photovoltaic devices. Therefore the development of PEA only perovskites are not the ideal solution to the low PCE issue. In fact, research is now focusing on exploring hybrid structures that integrate PEA-based 2D structures with 3D perovskites, forming mixed perovskite structures with new electronic and structural properties, which, ideally, will be able to enhance the good qualities of both structures. At the same time, it is possible to enhance the material's stability by surface passivation and compositional engineering, without compromising its stability. Finally, another alternative was found in introducing phenethylammonium salts (PEAX,X=Cl,Br,I) into

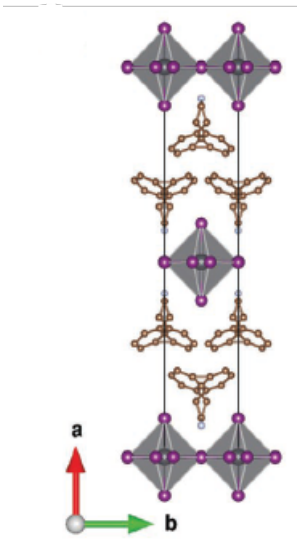

Figure 1.6: XRD results for thePEA_2SnI_4 perovskite showing disorder [14].

perovskite films as precursors with the aim of regulating the dimensionality and morphology of the films and subsequently forming 2D/3D perovskites. Indeed, the large organic groups of PEA will interact with the 6-fold coordinated tin octahedra and lower the dimensionality of the 3D perovskite but without creating a fully 2D one. This strategy has proven to be effective to address the problems for the optimization of perovskite films and the corresponding solar cells [11]. Furthermore, due to the generally faster crystallization process of tin, it is essential to optimize the fabrication methods for producing high-quality PEA_2SnI_4 films. Methods such as hot-casting, blade coating, and solvent engineering demonstrate potential for creating uniform, high-crystallinity films.
In conclusion, the constant progress in material synthesis, interface engineering, and stability improvement, indicates PEA_2SnI_4 as a promising candidate for the next generation of eco-friendly, high-performance optoelectronic devices and photovoltaic panels. Although by now it is primarily used in mixed perovskites, ongoing research into the properties and characteristics of this compound remains essential [15].

1.2 Aim of the Study

This work seeks to characterize single-crystal, tin-based perovskites, by a combination of solid state NMR (ss-NMR) and Single Crystal X-Ray diffraction (SC-XRD), aiming to provide a comprehensive understanding of their structure and dynamics. Indeed, XRD analysis is able to give information about the long range order of perovskites, but it

can become inaccurate when high structural disorder and fast molecular movements are involved, making it impossible to achieve a complete resolution of the crystalline structure. On the other hand, solid state NMR provides information about the local environment of the atoms in a molecule, as well as the nature of their dynamics in the crystalline lattice. For the purpose of this work, the PEA_2SnI_4 perovskite was synthesised using two different precursors: Tin Iodide (SnI_2) and Tin Oxide (SnO). The objective is to verify that the choice of the precursor has an influence on the structural order of the perovskite. This information is highly valuable for advancing research on the properties and behaviors of perovskites, as well as for improving the quality of materials used in optoelectronic applications.

Introduction: Solid State NMR

Solid State Nuclear Magnetic Resonance (ss-NMR) is a powerful spectroscopic technique used to investigate the atomic-level and three-dimensional structures of solid materials, and to examine the dynamics and interactions within them. It is based on the same principles of solution state NMR: the nuclei in the sample are positioned in a magnetic field and subjected to a radio-frequency (RF) irradiation in order to obtain a detectable signal. However, while molecules in solution NMR are free to move and rotate in a solvent, solid-state NMR deals with samples in a rigid or semi-rigid state, which leads to important differences both in the theory and the application of these two techniques [16].

2.1 The basics of ss-NMR

Nuclear magnetic resonance consists in the oscillatory response of nuclei with non-zero spins, to excitation by radio-frequency irradiation while subjected to a static magnetic field. The irradiation generates *resonance* which results in a detectable signal as the nuclei relax back to equilibrium [16]. This phenomenon is based on the properties of the quantum number I, which determines the number of energy levels (N) generated when a magnetic field is applied to the nuclei. The relationship between I and N is expressed by the following equation:

$$N = 2I + 1 \tag{2.1}$$

To understand why only nuclei with a non-zero spin are considered, one must simply substitute 0 as the value of I. This results in $N = 1$, which means that only one energy state is generated. Therefore, there is no possibility for power absorption by the nuclei, which means that no resonance phenomena can occur. Hence, nuclei where $I = 0$ are not useful for NMR purposes. On the contrary, when nuclei with $I = 1/2$, are considered,

the number of energy levels generated is 2. In fact when $I = 1/2$ the magnetic quantum number m can only assume two values: $m_1 = 1/2$ and $m_2 = -1/2$. Fortunately, almost every element in the periodic table possesses an isotope with spin $I = 1/2$, and can be used for NMR purposes.

The energy difference between the two levels is described by the equation:

$$\Delta E = \gamma \hbar B_0 \tag{2.2}$$

where γ represents the *gyromagnetic ratio* of the nuclei which is a property inherent to each isotope, $\hbar$ is the Boltzmann constant divided per π, and B_0 is the applied electromagnetic field [17]. Without the external magnetic field, the nuclei contained in a substance, spin with a precession motion around a randomly oriented axis with a rotational momentum μ. The purpose of B_0 is to align all the magnetic moments of the nuclei in its own direction, which corresponds to the **z** axis. However, the two energy levels (m_1 and m_2) that are generated by B_O, result in two different orientations of μ on the z axis: α ($m_1 = 1/2$), which corresponds to the low energy state and β ($m_2 = -1/2$) which is the high energy one. This phenomenon is outlined in Fig.2.1

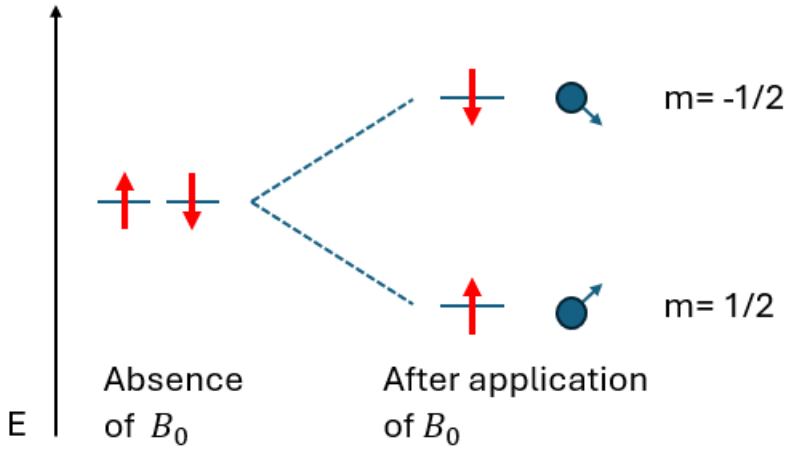

Figure 2.1: Schematic representation of the effects of the application of a static magnetic field to a nuclei with spin $I = 1/2$.

B_0 remains constant through the whole process and it is usually set around the order of 5 to 28T [16]. The sole application of B_0, though, is not enough to generate a NMR signal, meaning that the magnetic field is not able to induce a complete transition of all

the nuclei to the β energy level and consequently generate a resonance. The reason behind this is explained by the Boltzmann distribution:

$$\frac{n_1}{n_2} = e^{\Delta E/kT} \cong 1 + \frac{\gamma \hbar B_0}{kT} \tag{2.3}$$

Where n_1 and n_2 represent the population of the two energy levels. When only B_0 is applied, at room temperature, the difference in population is only slightly superior to 1, since ΔE is much smaller than the product kT. The transition between the two energy levels, and therefore the resonance of the nuclei will only occur if the system is perturbed from the equilibrium condition by applying a radio-frequency field along the x-axis or y-axis which oscillates at its own frequency. This frequency should equal the **Larmor frequency** which is given by the rate of precession of the magnetic moment of the nucleus around the external magnetic field.

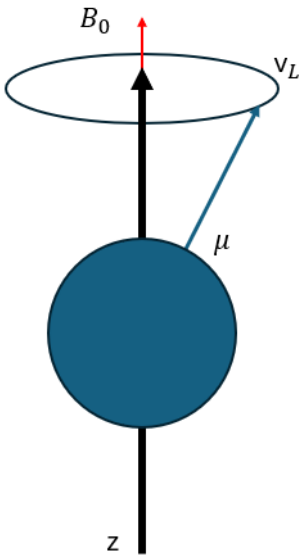

Figure 2.2: schematic representation of the precession movement of the nuclei around the z axis

This will allow the maximum power absorption by the system, which is now said to be in resonance, because there is an interaction of the magnetic component of the radiation with the nuclear magnetic moments, which also oscillate at the Larmor frequency. At this point the difference between the two energy levels becomes much greater, meaning that most of the nuclei are aligned in the same direction and occupy the β state, making the difference in population of the energy levels much larger.

The Larmor frequency is related to the strength of B_0.

$$\nu_N = \gamma B_0 \tag{2.4}$$

By combining equation (2.2) with equation (2.4) it is possible to rewrite ΔE as follows:

$$\Delta E = \hbar \nu_N \tag{2.5}$$

The transition frequencies of the nuclei lie in the radio-frequency regime of the electromagnetic spectrum, meaning low energy waves in a range of 1 to 1000 MHz.
The actual magnetic field experienced by the nucleus though, is not B_0. In fact it can be described as:

$$B_{eff} = B_0 - B_s \tag{2.6}$$

where Bs is the induced magnetic field, that is generated by the electrons surrounding the nucleus. Because of its nature, B_s changes depending on the chemical environment of the nucleus itself. This phenomenon generates the most important information that can be obtained by NMR spectroscopy: the **chemical shift**. Chemical shift represents the variation of the absorbed radiation and it allows to distinguish between nuclei of the same isotope that have a different chemical environment. To be quantified, there is the need of a reference substance to which the point-zero of the scale is assigned, usually being tetramethylsilane (TMS) in solution NMR. Since the chemical shift as described would depend on the value of the magnetic field, it is conventional to use the *relative chemical shift*, which is expressed as δ and it is the fractional difference of the frequencies of the interested nucleus over the TMS frequency. The chemical shift is influenced by a series of factors called *couplings* that originate from different causes, such as covalent bonds (spin-spin scalar coupling), inter-nuclear distances (spin-spin dipolar coupling) and quadrupolar couplings when $I > 1/2$, although the main focus of this work will be on dipolar nuclei [16], [17], [18].
All of the phenomena and features described above are characteristics of solution, as well as solid NMR. However, in solids, the interactions between nuclear spins are much stronger and not averaged out by rapid molecular motion as they are in liquids. Because of this, solution state NMR easily allows to distinguish nuclei of the same isotope that have a different local environment. On the contrary, when dealing with the solid state, the nuclei

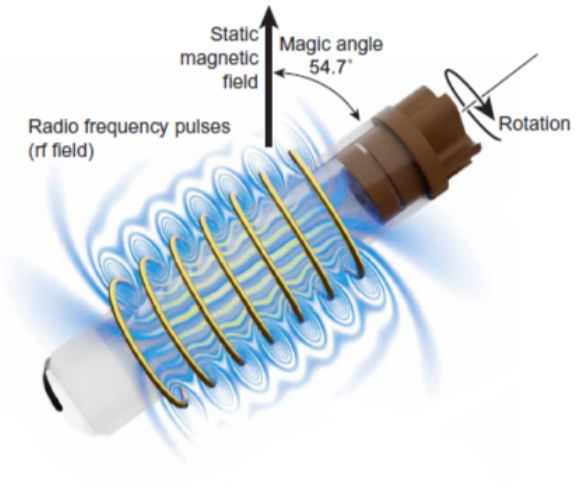

Figure 2.3: Representation of a spinning ss-NMR rotor subjected to the B_0 magnetic field and tilted by 54.7°[20].

are subjected to anisotropy due to the rigidity of the structure. This means that the spin interactions vary based on the sample's orientation relative to the direction of the magnetic field. One important type of anysotropy is called *chemical shift anisotropy* (CSA) and it arises because of the orientation dependence of the local magnetic environment around a nucleus. This results in a spread of resonance frequencies, leading to broad NMR signals, even for nuclei that share the same local environment. The line broadening due to CSA, is called "inhomogeneous". Another type of anisotropy is given by heterogeneous dipolar couplings, where the vicinity of two different isotopes will generate small magnetic fields that influence each other, resulting in a broadening of the signal of each nucleus, making it impossible to highlight the interactions between heteronuclei [17]. In order to solve these important issues, various high-resolution techniques have been developed which are capable of removing the anisotropy of spin interactions, enabling the acquisition of resolved spectra [19].

Magic Angle Spinning

Magic Angle spinning is a revolutionary technique that allows for most of the anisotropic effects to be eliminated. It is achieved by tilting the rotor that contains the sample by an angle of 54.7° from the static magnetic field, as showed in Fig.2.3. The basic concept of MAS is rooted in the orientation dependence of these interactions relative to the external magnetic field, which are strongly dependent on the angle θ between the internuclear

vector, or principal axis of the chemical shift tensor, and the magnetic field B_0. When $\theta = 54.7°$ the chemical shift anisotropy is averaged to zero because of its dependence from the factor:

$$3\cos^2\theta - 1 \tag{2.7}$$

The process of spinning the sample at this angle significantly narrows the NMR spectral lines, resulting in higher resolution and better-defined peaks. The spinning frequency must be fast enough to effectively average out the anisotropic interactions, typically in the range of several kHz to tens of kHz. Today, MAS rates of 5–100 kHz are accessible using cylindrical rotors with diameters ranging from 0.7mm to 7mm. This allows for detailed analysis of the atomic-level structure and dynamics of solid materials, which would be challenging to achieve with static samples. Moreover, the speed at which the MAS is set, is a factor of extreme importance, since in order to obtain a single line at the isotropic chemical shift, the rate at which the sample is spinning should be greater of a factor or 3-4 compared to the anisotropy [21]. If the spinning is lower, a set of spinning sidebands will be generated in addition to the expected peak. Spinning sidebands are sharp lines separated by a distance corresponding to the spinning speed and they radiate out from the isotropic chemical shift line, which is not necessarily the most intense line, although it is the only one that does not change position depending on the spinning speed. This feature is the only reliable way of identifying it. In Fig.2.4 three different spectra are depicted, highlighting the differences between static and non static spectra [22]. Another factor to consider when adjusting the spinning speed is that depending on the atoms examined and on the experiment performed, the optimal speed of rotation of the MAS can differ. For instance, when considering carbons ^{13}C, aliphatics present a small CSA, which means that lower speeds are enough to eliminate the anisotropy, while on the other hand, carbons forming multiple bonds will require a higher speed to average their CSA. Finally, since B_0 has a direct influence on the CSA, for stronger applied electromagnetic fields, much higher MAS rotational speeds are.One important consequence of using MAS is that it doesn't make any distinctions between all of the information-rich anisotropic chemical shift and dipolar interactions, therefore many radio-frequency pulse sequences have been programmed to reintroduce only the desired spin interactions, without negatively impacting the spectral resolution. From this basis the most relevant ss-NMR experiments can be carried out.[16]. The calibration of the magic angle is an extremely important and critical step, since even

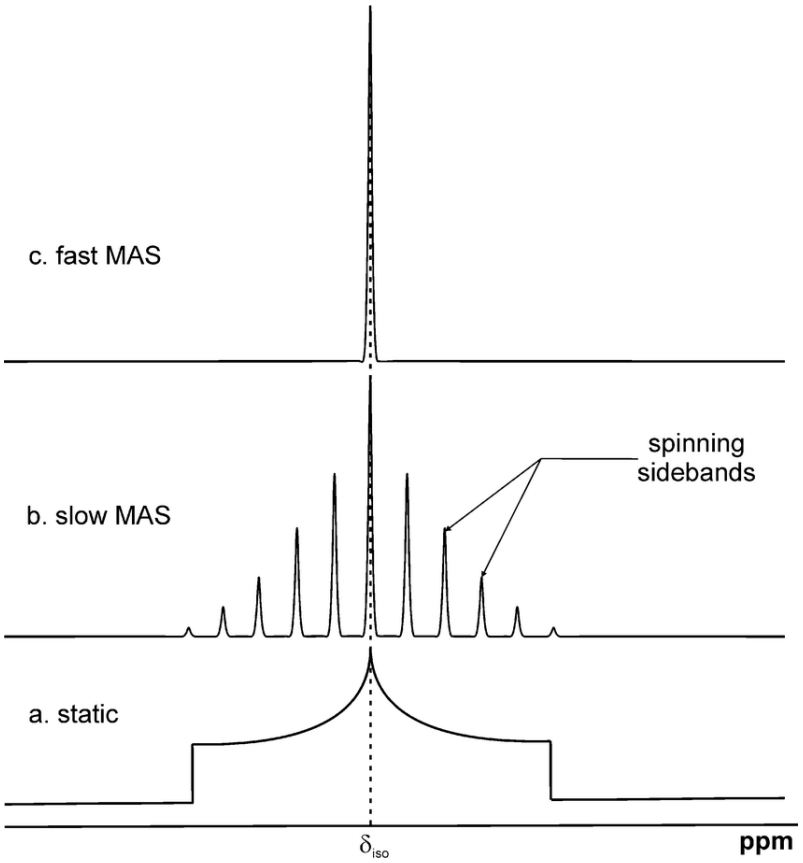

Figure 2.4: effects of MAS spinning at different rates on the same sample [22].

a decimal error in the calibration can give a signal broadening of a few ppms, which should not be neglected.

High Power Decoupling

Because heteronuclear coupling among X and ^{1}H also strongly contributes to line broadening issues, another important technique is the *dipolar decoupling* or *high power decoupling (HDP)*, where decoupling is used with reference to the heteronucleus. It consists in continuously irradiating the sample with ^{1}H radio-frequencies, while observing the X nuclei. This way, the ^{1}H spins precess around an axis in the transverse plane and gradually bring the z-component of the ^{1}H magnetic moment to zero. This technique allows ^{1}H spins to change their energy states with a higher velocity compared to the heteronuclear dipolar interaction frequencies, which eliminates the local dipolar fields on the heteronucleus. The NMR experiments for which this technique is needed, the irradiation takes place only during acquisition, to avoid energy waste and overheating of the sample [17].

Cross Polarization

Another problem that arises when acquiring NMR spectra of solid samples, is the presence of some nuclei that have low natural isotopic abundance and low gyromagnetic ratio, which are called *rare* nuclei and will give weak signals if directly irradiated, making it difficult to obtain clear spectra, both ^{13}C and ^{15}N are part of this class of nuclei. To solve this, a technique called Cross Polarization was developed, where the polarization is transferred from more abundant and higher-sensitivity nuclei, typically ^{1}H, to the target nuclei. This is achieved by applying a series of RF pulses to both sets of nuclei simultaneously, allowing the strong spin polarization of the abundant nuclei to be transferred via dipolar couplings to the less sensitive ones, by matching their spin lock conditions, meaning their energetic levels. This results in a resonance of the two nuclei, and consequently, in the enhancement of the signal intensity of the low-sensitivity nuclei, leading to better a signal-to-noise ratio in the resulting spectra. The matching of the energy levels is called **Hartmann-Hahn** condition and it is described by the following equation:

$$\gamma_X B_{1X} = \gamma_H B_{1H} \tag{2.8}$$

where γ_X and γ_H are the gyromagnetic ratios of the heteronucleus and the proton, respectively, and B_1 is the RF pulse that is applied on the nuclei. This condition takes place when the RF pulse on the heteronucleus is bigger than the pulse on the proton of a factor equal to the ratio of gyromagnetic constants γ_H/γ_X. In the case of ^{13}C, B_{1C} is 4 times stronger than B_{1H}. The final effect is an increase in the signal intensity of the diluted nucleus. A schematic representation of the CP pulse frequency is illustrated in Fig.2.5. The Hartman-Hahn condition needs to be retained for a determined time called *contact time* τ_c in order to maximise the signal. The contact time varies between samples because it must remain within certain limits; exceeding these limits can lead to signal loss due to nuclear relaxation. Regarding the speed of spinning, a straight increase of the speed would not necessarily improve the resolution, on the contrary, in this case, a too high velocity has a negative impact on the decoupling of the nuclei, hence it generates a worse signal overall.

On the other hand, naturally rich nuclei have strong homonuclear dipolar coupling, therefore high resolution spectra are not easy to obtain with basic experiments, and there is

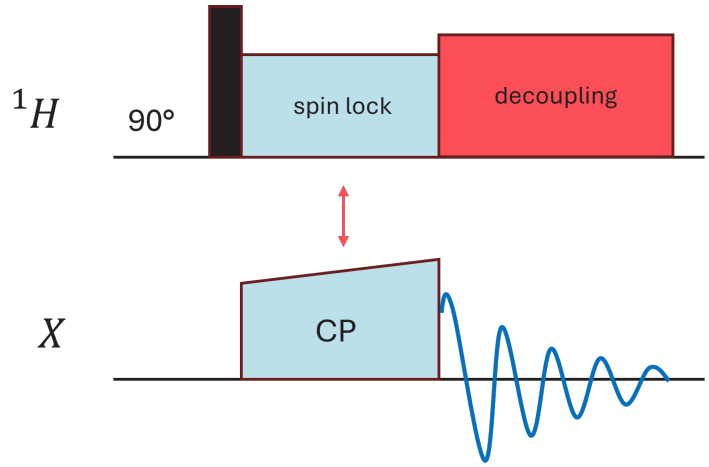

Figure 2.5: Schematic representation of CP pulse sequence

the need to apply high-resolution and more sophisticate experiments. Specifically, high speed spin will act on homonuclear decoupling.

2.2 Ss-NMR on perovkites

When working with solid state materials, such as crystals of powders, the use of X-ray diffraction (XRD) crystallography can be the a great choice in many cases, since it provides a vast range of information and it can analyze a wide variety of materials, including perovskites. But when the disorder of a molecule is high, or the long range crystal order is lost, this technique can become inaccurate and not entirely reliable. Generally, XRD is highly dependent on the presence of hydrogen bonds, which have been only minimally explored in MHPs. This limits the effectiveness of the technique [23], [24].

Among the vast range of experimental methods that utilize physical phenomena to provide structural information, ss-NMR spectroscopy holds a crucial position. In fact, solid-state nuclear magnetic resonance has proven to be an indispensable tool for gaining insights on perovskites, as it has been used to investigate short range structural environments like the composition of perovskites and the eventual incorporation of ions in the lattice, as well as to study their local dynamics, and their overall stability [23].

These factors are extremely relevant for a deeper understanding of the relations between structure and function in existing perovskite materials, as well as beneficial in the development of novel materials. At the moment, the use ss-NMR to research these compounds has been limited, since it is not a simple technique that can be easily managed by the oc-

casional user. It needs dedicated and complex equipment, which can be highly expensive: from the high power of the radiations to specific instrumentation and set-ups that are built for ss-NMR use only. Nevertheless, these are common issues faced with high technological techniques, and the power, sensibility and flexibility of ss-NMR definitely outshine its disadvantages, hence it is fundamental to work for further intensification of research on perovskites and their interesting properties through this fascinating technique. Among the many advantages of ss-NMR that should be considered, is its unique selectivity that allows to differentiate chemically distinct environments on the basis of the chemical shift [23].

One of the earliest and most thoroughly examined topics in ss-NMR studies of hybrid halide perovskites is the dynamics of their components, which are also essential for the objectives of this work. Other than dynamics, the study of the chemical composition of a perovskite is also a crucial factor for the improvement of the optical properties and the stability of these materials. For this reason, ss-NMR can be used to analyse the local environment of a nuclei in the perovskitic structure. In fact, through this technique it is possible to distinguish the different nuclei coordination, thus, to recognize whether an ion introduced in the perovskite formulation has been correctly incorporated in the lattice or it has undergone phase segregation forming non-perovskitic structures. As a result, ss-NMR can also be used to investigate the presence (and extent) of disorder within a molecule when it has integrated specific moieties [25]. The examination of the dynamics and structural environment of a nucleus can be directed toward understanding the properties of the entire material or focused on a smaller section. In MHPs most of the research has been carried out on cations that occupy the A site. In fact, they are able to influence the lifetime of the charge carriers and the shape of the electronic band structure, which can be modulated by molecular rotations. Meaning that they have a direct impact on the crystal structure of perovskites and on their optical properties.

A site cations

When characterizing the organic or inorganic cations that occupy the A sites of perovskites, the main questions to be asked are if they are correctly incorporated in the perovksite, how different cations mix within the perovskite phase, what is their orientation and distribution, and how this can influence the physical structure of the perovskite,

and thus, the properties of the material itself. Various works through the years have been dedicated to the use of ss-NMR with the objective of answering these questions and many more.

There are 3 main cations that are known to be used in 3D lead halide perovskites, which are also the most common ones for tin-based HPs. Two organic cations: Methylammonium [$CH_3NH_3^+$] and Formamidinium [$NH_2CHNH_3^+$], and the inorganic Cesium [Cs^+]. Their geometries allow them to fit correctly into the 12-coordinate A sites [24]. These cations can be used singularly to form perovskites, but to obtain high performance perovskite solar cells and LEDs, the best strategy is to combine them in different concentrations, so that their own flaws are compensated by the other cations' strengths [24]. When it comes to 2D perovskites, the types of cations that can occupy the A site have different requirements. Ss-NMR spectroscopy is also increasingly useful for elucidating their role in perovskite materials. The dynamics of organic cations can be extracted from relaxation times in different 2D structures, which provide important information about crystal rigidity [24].

Another fundamental aspect of the study of A-cations, regards the insertion of moieties and passivating agents inside the lattice of perovskites. In fact, as already explained thoroughly in Chapter 1, one of the main problems of perovskites, is their instability under atmospheric conditions due to reactivity with oxygen and water [26]. Hence, to improve their performance and chemical stability, small adjustments of the composition and the structure of MHPs have been proposed during the years. Often, this problem is being faced by incorporating layers of organic cations in hybrid perovskites to form 2D perovskites, hence by changing the composition of the A site. This is a crucial point in perovskite research and their development process. In fact it is not an easy task to understand how and if the perovskite precursors have actually been incorporated in the lattice. Since, during the process of production of perovskite devices, many different chemical processes take place, and the addition of ions in the precursor solution can influence many aspects of the final device, such as morphology and crystal quality, but without being actually incorporated in the solution. Hence, any change in efficiency of the devices, is not a real proof of the incorporation of the added ions in the lattice. For this reason, employing ss-NMR to study the incorporation and distribution of additional A-site cations within the perovskite structure is highly significant. The structural changes caused by these

alternative cations are subtle, making XRD less effective for studying such materials. By exploiting the results obtained by this work, for instance, it would be possible to understand how and where, eventual passivating agents, would be incorporated in the perovskite lattice. But before that, it is mandatory to have a complete background of the single cation perovskites, their features, their problems and their behaviours in solid state NMR analysis, in order to perform reproducible results and avoid creating artifacts that would distort the final results. As a matter of fact, for this work, two tin halide perovskites were synthesised: one 3D $FASnI_3$ and one 2D PEA_2SnI_4. The state of the art on the characterization by ss-NMR of the A-site cations of the mentioned perovskites is described below.

State of the art: Formamidinium

Formamidinium is one of the most used cations of the A site for 3D perovskites. For this reason it is fundamental to understand how well it can be mixed with other cations and the effect that it has on the material and its properties. Most of the studies carried out regarding Formamidinium take in consideration lead halide perovskites, in fact, the first NMR study of mixed A cation perovskite materials was performed by Kubicki et al. [27] by incorporating both methylammonium (MA) and formamidinium (FA) ions in the structure of a lead perovskite and subsequently investigating their dynamics. The proof of FA incorporation inside the perovskite lattice was the changed chemical shift of the ^{13}C of MA upon the addition of FA. This creates a fundamental precedent in perovskitic analysis through NMR, and a great starting point for our research. While if the focus is to be shifted on tin perovskites, another study by Kubicki et al. can be taken in consideration [28], where the local structure and dynamics of mixed-cation, tin-based perovskites are analysed through ^{119}Sn NMR spectra instead of ^{13}C and ^{1}H. For the study, three different halogen anions (I^-, Cl^- and Br^-) and the three main A-site cation for 3D perovskites (FA, MA and Cs) are used to synthesise mixed-halide and both mixed-cation perovskites and single-cation ones. In this case the research is more focused on the effects of the different halogen used, and the results of the analysis are not extremely relevant regarding the dynamics of the A-site cations, but it is proven that the shape and chemical shift of the ^{119}Sn signal, change depending on the coordination, thus the composition, of the perovskite. Moreover it is a great reference to where the tin peak should be positioned

on ss-NMR spectra when coordinated to FA or Cs.

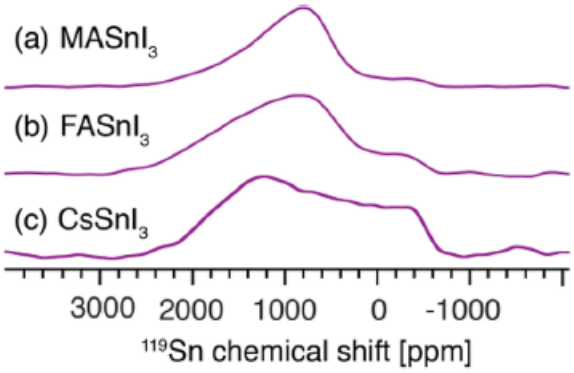

Figure 2.6: ^{119}Sn spectra of three perovskites recorded in static conditions (b) and with MAS=12kHz[28].

State of the art: Phenethylammonium

Phenethylammonium is an organic aromatic cation used to form 2D perovskites of the RP type, to form a material with the general formula PEA_2BX_4. Until now, the research has been focused on lead halide perovskite containing phenethylammonium. Important studies on the dynamics of this A-site cation in 2D Lead halide perovskites were carried out by Ueda et. al [29]. With the objective of studying the orientation and movements of the molecule in the organic layer and see if the halide ion of choice would make a difference in the dynamics of the A cation. This study concludes that depending on the halide anion used, the disorder of the organic layer, changes. This can be extrapolated from the ^{13}C spectra of the three perovskites, that show a different splitting of the aromatic signal for each perovskite. In the presence of I^-, all of the aromatic carbons that do not lie on the symmetry axis correspond to 1 peak. This does not happen for Br^- and Cl^-, where the peaks are respectively split into two and three. This can be associated to a different orientation of the PEA cation, hence to a disorder in the lattice of the materials. The study gives a general picture on the dynamics of phenethylammonium and how "easily" they can be influenced. It can be taken as a reference when studying how this cation would behave if the B-site cation is changed to tin. In this work, the dynamics of phenethylammonium in tin iodide perovskites are studied thoroughly, to understand if even different precursor can influence its mobility and orientation. In general, since they are a relatively new subject, not much work has been done on the synthesis and characterization of 2D perovskites. Specifically, at the time of writing, there is no characterization of 2D tin perovskites

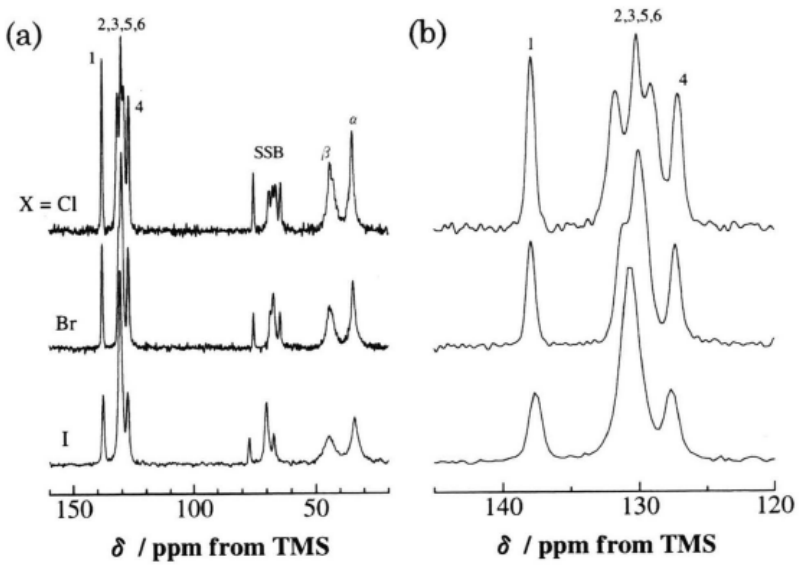

Figure 2.7: ^{13}C spectra of PEA_2PbX_4 perovskite showing the influence of the different halides [29].

with ss-NMR. Nevertheless, they are generating more and more interest in the research, because of their broad range of potential applications, mainly in lasers and transistors [30].

Conclusions

ss-NMR is a great tool to analyse and provide information on the structure and dynamics of perovskites. This is fundamental to help develop more stable and better performing perovskites. Since a successful incorporation of a material can be crucial to the correct functioning of a perovskite-based device, and on the contrary, if phase segregation takes place, the stability could strongly suffer from it. Ss-NMR on perovskites is also used to analyse degradation patterns, in ordet to make it easier to understand if a signal anomaly is given by degradation or not. Moreover, a good understanding of the decomposition mechanisms is essential for developing more stable alternatives of perovskites.

Finally, as most of the ss-NMR studies performed on perovskite materials until now, have predominantly concentrated on elucidating structural characteristics or assessing material stability, it is crucial to start developing NMR protocols and investigations that are able to correlate spectral data to the material performance. Since the performance is definitely a central factor for application of perovskites in LEDs and photovoltaic (PV) devices. To achieve this, studying perovskite materials under real operating conditions, such as during illumination or the application of voltage, will likely be highly beneficial [25].

2.3 Single Crystal X-Ray Diffraction

Crystal X-ray diffraction (XRD) is a powerful and widely used analytical technique for determining the atomic planes and molecular structures of crystalline materials. This method exploits the constructive interference between monochromatic X-rays and the periodic lattice of a crystalline sample, to obtain information about the crystalline solids. In fact, by analyzing the diffraction patterns generated when X-rays pass through a crystal, it is possible to determine the positions of the atoms in the lattice, the distances between them, and the angles at which they are bonded, and therefore to determine the *disorder* of a crystalline structure. XRD setups consist of a X-ray source, the sample, and the X-ray detector, as depicted in Fig.2.8. The X-ray generator is given by a cathode ray tube, usually made of Copper (Cu) or Molibdenum (Mo), after being generated, the signal is filtered to produce monochromatic radiation, and then directed toward the sample. The source remains static while the sample is rotated on an axis, as is the detector. Monochromatic X-rays are generated when accelerated electrons hit a target (usually a metal) and cause electronic transitions on that material. After excitation, the electrons return to the ground state, producing emission of photons. The energy of the generated particle lie in the range of X-ray, which is between 10^2 and $10^5 eV$ [31]. The constructive interference needed to generate a detectable signal can occur only when the Bragg's law conditions are satisfied:

$$n\lambda = 2d \sin\theta \tag{2.9}$$

Here, n represents an integer λ is the wavelenght of the X-rays generated, d is the distance between the planes of the crystal and θ is the angle of incidence. What happens in practice is that when a crystal is subjected to a monochromatic ray beam, the X-rays get scattered by the planes of the atoms in the crystal, creating a diffraction pattern, which is only detectable at certain values of θ. The constant rotation of the crystal in fact, allows for the detector to systematically record the angles and intensities of the diffracted beams. This way, all possible diffraction directions of the material's lattice should be obtained due to the random orientation of the sample. The collected diffraction pattern is converted into a 3D dataset of intensities and corresponding diffraction angles. Finally, by using specialized software, the diffraction data are analyzed to solve the phase problem, and electron density map are constructed. From the map, the positions of the atoms are

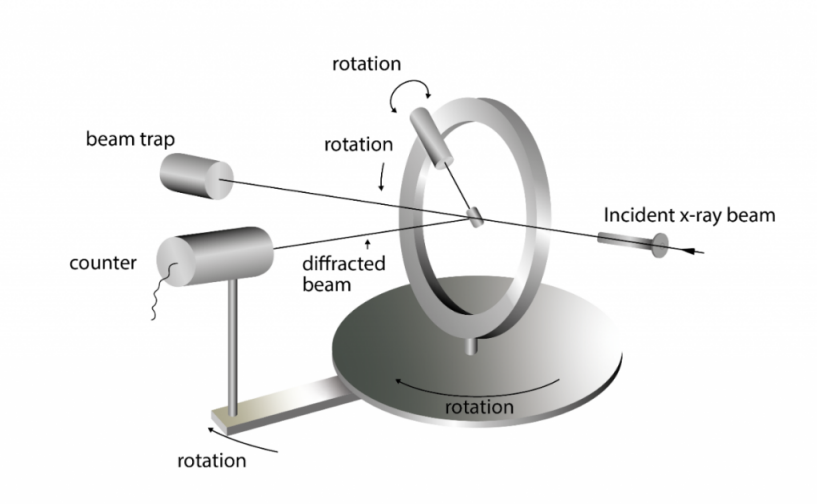

Figure 2.8: schematic representation of an XRD set up [33].

determined, and the final structure of the crystal is refined. Each substance has its own distinct diffractogram [32].

There are two main types of XRD experiments: Single Crystal XRD (SC-XRD) and Powder XRD. They both work with the same theoretical principle, but for the purpose of this thesis, only single crystal XRD will be discussed. The patterns obtained by Single Crystal XRD are given by single dots scattered across the area of analysis, where each spots indicates an intersection of diffracted X-rays. The information contained in the signals can be related to their location and intensity. The former contributes in assessing the angle of diffraction and therefore, the relative orientation of atoms, while the intensity offers details about electron density. Among the most important information that can be derived by SC-XRD analysis there are also:

- Symmetry and Space Group: XRD reveals the symmetry of the crystal structure and the space group, which describes the symmetry operations (e.g., rotations, reflections) that relate equivalent points in the crystal.

- Lattice Parameters: XRD determines the dimensions of the unit cell, the smallest repeating unit in the crystal lattice.

- Atomic Positions: The technique allows for precise determination of the coordinates of atoms within the unit cell.

- Phase Identification: For polycrystalline materials, XRD can identify different phases present within the sample, based on characteristic diffraction patterns.

2.3.1 SC-XRD on perovskites

XRD can be an extremely useful tool for the study of perovskites, as it provides important information regarding the structure of the crystalline sites, which have a direct influence on the functional properties of these materials. Among the advantages of XRD, it can be highlighted that it is a non destructive technique, which also means that the materials can be studied without any alteration taking place on their structure. Moreover, crystal XRD is able to confirm the perovskite phase by providing the structure of the unit cell and its parameters. This can be helpful even to detect the presence of defect or impurities. Eventually, it can also be used to monitor the phase transition of perovskite crystals, which could be influenced by a change of temperature, an increase in moisture or in the case of tin-based perovskites, a long exposition to air, hence it is fundamental to provide information about the stability of the material. Finally, for perovskites, having detailed information about thr atomic arrangement of the lattice, is crucial for understanding how structural parameters can affect the electronic properties and thereby the overall efficiency of the material.

However, as any characterization technique, also XRD has its limits. Indeed it is quite sensitive to disorder, and because perovskites often present disorder, due to mobility or to the actual arrangement of the atoms in both the inorganic and organic phases, XRD may have difficulty resolving fine structural details of these materials. Finally XRD is a long range technique, which works great for resolving the bulk of the material, but it can lack in highlighting smaller difference. Thus, combining Crystal XRD with solid-state NMR is highly beneficial, as this integrated approach enhances the resolution and understanding of perovskitic structures, offering a more comprehensive characterization of these complex materials.

Materials and Methods

3.1 Synthesis of Perovskites

For the purpose of this work two hybrid inorganic-organic perovskites were synthesised: $FASnI_3$, which presents a 3D structure, and PEA_2SnI_4, which is a 2D perovskite. Both perovskites were synthesised starting by two different precursors: SnO and SnI_2.

3.1.1 Synthesis of $FASnI_3$

Use of SnI_2 as precursor

The Synthesis of Formamidinium Tin Iodide crystals was carried out under nitrogen to avoid the degradation of tin. The synthesis is a modified version of the one carried out by Kahman et al.[34]. Here 0.206g of Formamidinium Iodide [FAI] per 1.20mmol and 0.373g per 1mmol of SnI_2 were weighted inside the glove box directly in a double-necked flask. The flask was then transferred out of the glove-box and connected to the nitrogen pipe in the Schlenk set up, while being positioned on a heating plate equipped with a Temperature ramp. A picture of the setup is shown in Fig.3.1a Then a solution of HI/H_2PO_3 1/1 was prepared by mixing 3.25mL of both acids in a measuring cylinder. Before inserting the solution in the flask, the temperature of the plate was raised to 100°C. Finally the solution was slowly added to the flask under stirring, while temperature was raised up to 120°C. After dissolution of the powders, a clear yellow solution was obtained. The stirring was turned off and the temperature ramp was activated. The ramp was set to decrease the T to 25°C in steps of 6 $^{\circ}\mathrm{C\,h^{-1}}$. After a few minutes, the first black crystals were formed, they were left in the flask until reaching of the target temperature. When temperature decreased to the set value, an orange coating-like layer was formed on top of the liquid

phase, which could indicate the formation of by-products. As $FASnI_3$ is a 3D perovskite, the crystals had a very well defined cubic shape, the colour was black and iridescent.
The workup was carried out under nitrogen flux to avoid oxidation. A fritted funnel was set up on a vacuum flask which was connected to a portable vacuum pump. A small plastic funnel was connected to nitrogen and set over the fritted funnel, to allow a constant flux even during the workup. The crystals were quickly transferred from the flask to the fritted funnel. They were then washed with refrigerated EtOH and diethyl-ether Et_2O for three times each. Then the crystals were transferred to a sheet of filtering paper and separated to check if the solvent was completely eliminated. Finally they were set in a single-necked flask under vacuum for about an hour and then transferred inside the glovebox.

Use of SnO as a precursor

The same reference was used for the synthesis of the same perovskite starting from SnO and again FAI. A flask was inserted inside the glove-box and 0.135 of SnO and 0.206g per 1.20mmol of FAIn were weighted directly inside it. The synthesis procedure is the same as the one starting from SnI_2. The crystals obtained had a more defined cubic shape and no orange phase was formed above the solvent. The workup was carried out using another procedure to allow better drying of the crystals. The workup procedure is identical to the one mentioned in the previous paragraph. A picture of the crystals under a microscope is reported below in Fig.3.1b

3.1.2 Synthesis of PEA_2SnI_4

Use of SnI_2 as a precursor

Initially, 0.633g per 1.7mmol of Tin iodide were weighted in a double-necked flask inside the glove-box, then 0.42mL of phenethylammine were measured in a beaker and finally 10mL of a HI/H_2PO_3 1/1 solution were prepared. Then the weighted SnI_2 was carried out of the glove box and fixed to the Schlenk line under continuous N_2 flux to avoid degradation. The flask was positioned on a plate. 2mL of the acidic solution were added under fast stirring to the powder, then T was raised to 100°C. Phenethylammonium was drawn from the beaker and added to the flask drop by drop. Finally the last 8mL of the acidic solution were gradually added to the flask to allow the dissolution of the powder.

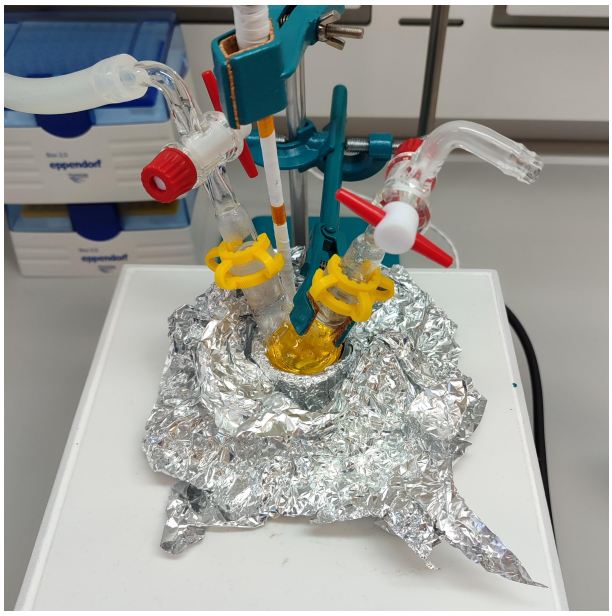

(a) set up for $FASnI_3$ syntheis on the heating plate

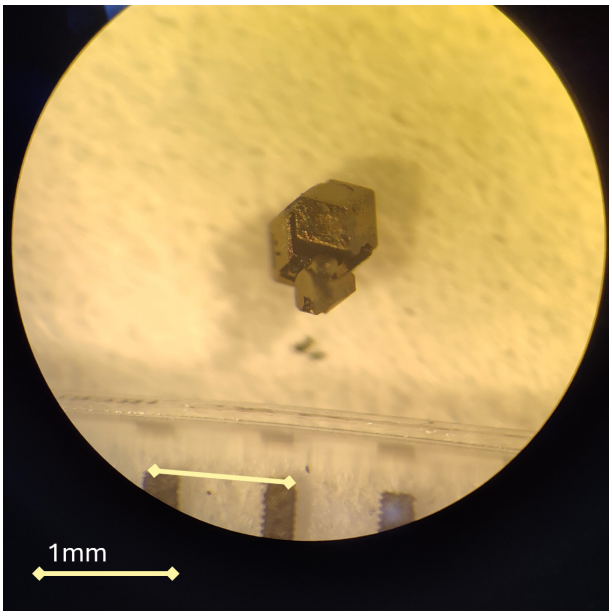

(b) Crystal of $FASnI_3$ under a microscope

To avoid that the precipitate would take up the whole solution and form a single block of material, 1mL of HI/H_2PO_3 1/1 were added to the flask and the solution was covered with aluminium foil and kept heated and stirred until complete dissolution of the powder. The solution turned into a clear yellow colour, and was set to rest for at least 3h.
The obtained crystals were flake shaped, since PEA_2SnI_4 is a 2D perovskite. They were light and fragile, the colour was black with red and purple iridescent shades.
The purification of the crystals was carried out using the same set up mentioned for the workup of the $FASnI_3$ from SnI_2. Again, the crystals were washed with refrigerated EtOH and Et_2O, then separated manually on a piece of filtering paper and finally set under vacuum for an hour. They were then transferred in a vial and inside the glove-box to prevent degradation.

Use of SnO as a precursor

The procedure is very similar to the one described in the previous paragraph. Here, 0.223g of Tin Oxide SnO were weighted inside the glove-box. The flask was then positioned on a plate and under continuous N_2 flux. Then, 0.42mL of PEA were measured in a beaker. 10mL of the HI/H_2PO_3 1/1 solution were prepared. The temperature of the plate was brought to 100°C under spinning. Finally, 2mL of the acidic solution were added to the flask. After SnO was dissolved, 2mL of the same solution were added to the measured

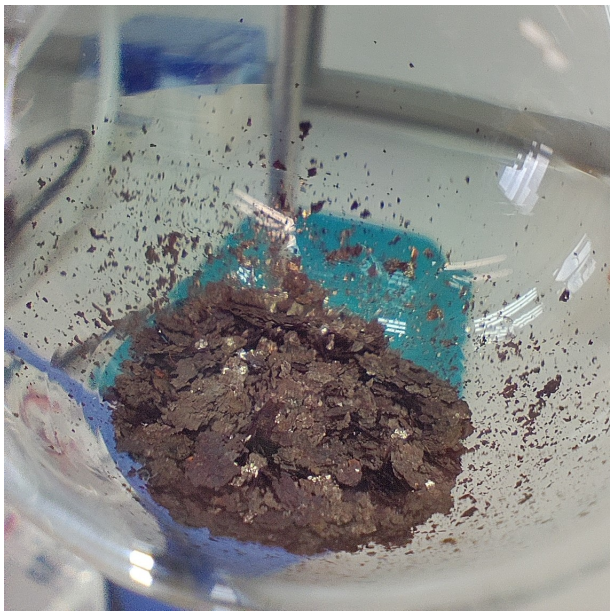

Figure 3.2: Crystals of PEA_2SnI_4 starting from SnI_2 as a precursor

phenethylammine, which precipitated immediately as phenethylammonium iodide. It is, therefore, fundamental to keep the solution heated to allow further solubilization of the precipitate. At this point a Pasteur pipette was heated and the solution was drawn and added to the Tin oxide one. The remaining 6mL of the acidic solution were gradually added to the flask. Since the powder was not yet completely dissolved, another 5mL of HI were added directly to the flask. The solute was finally dissolved and the solution turned into a clear yellow colour. Again the solution was set to cool down without a ramp for at least 3h and covered with an aluminium foil jacket. The crystals formed were again flake shaped, with a slightly larger area than the ones from SnI_2. The colour was black with red iridescent shades. The workup procedure is the same as described in the previous paragraphs.

3.2 Sample preparation

ss-NMR

To allow the characterization of single crystal perovskites by solid state NMR, the sample needs to be inserted in a rotor with a 1.9mm diameter. In order to do so, the rotor must be opened from the top side, where the helix is. Than the rotor and the relative packing kit, depicted in Fig3.3, are inserted in the glovebox, where the crystals are conserved.

Once all of the necessary tools are in the glove-box, the crystals of choice are grounded with an agate pestle in the mortar of the same material. After the crystals have been turned into powder, the rotor is set inside the suited funnel and the powder is inserted in very small quantities. After every single insertion it is important to press the powder with enough strength that turning the rotor upside down it won't fall from the inside. At the same time, the rotor is extremely delicate, so it needs to be managed with care in every instance. The powder is inserted and pressed with a small piston until the red groove on the piston coincides with the upper edge of the rotor. At this point, the rotor is full and the upper cap can be reinserted. The rotor is carried out of the glove-box and ready to be inserted in the MAS probe.

(a) 1.9mm rotor filled with PEA_2SnI_4 powder

(b) Tool kit for ss-NMR rotor packing and un-packing

Figure 3.3: Pictures of a rotor and the relative toolkit

XRD

The sample preparation for Single-crystal XRD can stare from both wet and dry crystals. For both these methods, a glass slide needs to be filled with vaseline or oil. The reason for this procedure is threefold: itcan help to avoid the degradation of the crystal, it favors the 3D vision of the crystal under the microscope, and it avoids that the crystal moves around on the glass to help with its picking.

When the crystals have been conserved in the mother solution, they can be scooped from the flask and transferred on the glass slide covered in oil. While for the crystals conserved in dry conditions, it was found that it is better to insert the slide covered in oil directly in the glove-box, so that the crystals won't be degraded by exposition to air. After positioning the crystals on the slide, the procedure is the same for both cases. With the help of a microscope, a few single crystal with uniform and well-defined edges are chosen

and mounted on different small glass nails, one for each crystal chosen. The sample is then covered again in vaseline to avoid that the crystal detaches from the mount. Finally, the nail is positioned on the goniometer inside the instrument and measurments can take place.

3.3 Characterization: ss-NMR

Solid-state NMR, as previously noted, is a highly valuable technique for analyzing and gaining insight into the behavior and structure of crystalline materials like perovskites. This section aims to offer a concise summary of the functioning and purposes of NMR experiments.

To briefly summarize the points covered in the introduction of this work, when a solid sample is subjected to a static magnetic field B_0, most nuclear spins align parallel to the magnetic field and orient along the z-axis. Then, the nuclei are exposed to short RF pulses since NMR instruments are equipped with a radio-frequency generator. If RF coincides with the Larmor frequency, the pulses will be able to rotate the bulk magnetization of the sample's nuclei by a specific angle. Pulses are generally described by this angle of rotation, also called *flip angle*. The manipulation of the orientation, intensity and sequence of the oscillating pulses that are applied to the sample is as what distinguishes different NMR experiments from each other, giving them unique goals and purposes. Finally, after the excitation of the nuclei, the acquisition of the RF signal generated by the nuclei takes place. The NMR signal is recorded in the form of an exponentially decaying sine wave, which is called *Free-induction decay* (FID).[35] The FID is then translated in a spectrum of intensity in function of ppm, so that the recorded peaks can be easily visualised. In the next paragraphs, the main experiments used during the development of this work are described.

3.3.1 Instrument

Solid state NMR measurements were performed on a Bruker Avance NEO WB with wide bore magnet (89mm) operating at a ^{1}H frequency of 400MHz. The chemical shift for all nuclei was referenced to the ^{13}C signal of adamantane at 38.46 ppm. The CP-MAS probe that was used for the characterization is a 1.9mm probe with a spinning frequency

that ranges from 5 up to 42kHz, which is among the highest spinning rate that can be achieved by ss-NMR instruments. The 1.9mm rotors employed, are made of zirconia with VESPEL turbines. The temperature was controlled with a Bruker BCU II chiller, with a range from 268 to 353K.

3.3.2 Experiments

One Pulse

The experiment **One Pulse** is the most simple pulse sequence that can be performed in NMR analysis. It consists in a single 90° pulse that is applied to the sample, which is then, immediately acquired. A simple diagram of the experiment is depicted below in Fig.3.4.

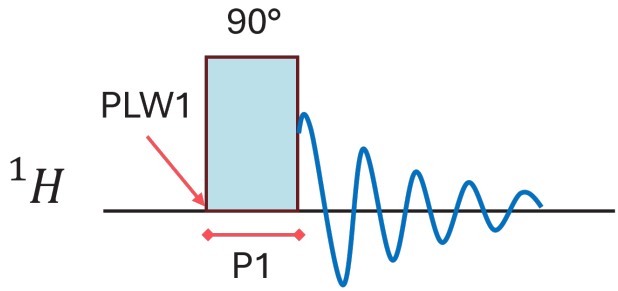

Figure 3.4: Description of One Pulse, pulse sequence

This experiment mainly work with abundant nuclei, such as ^{1}H which easily resonates with just one single pulse, but it is not a very high-resolution experiment. Being a relatively easy experiment, the pulse program is already tied to the parameter set. The main parameters that should be considered for this experiments are:

- P1: it is the 90° *Pulse Width*. At a given power level, it is the pulse width causing spins to flip of 90°. In simpler words, it corresponds to the duration of the pulse applied to the particular sample, it is therefore measured in seconds (s)
- PLW1: it is the power of the pulse applied to the nucleus 1, namely the proton. It is measured in Watts (W) and it is a fundamental parameter for most of the experiments of the solid state, since for different nuclei, different power of the pulse is required to achieve the wanted flip of the magnetization.[36]

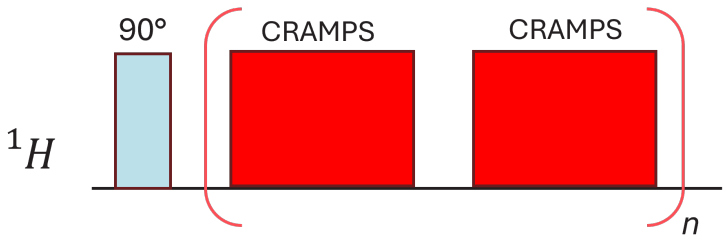

Figure 3.5: Pulse sequence of wpmlg, where CRAMPS sequences are repeated n times, during acquisition of the signal

WPMLG

Although ^{1}H has a 99% abundance, proton NMR in solids is not that common. In fact, as previously mentioned the one pulse experiment does not present high resolution, and instead gives wide and at times featureless spectra. This is manily due to the presence of strong homonuclear coupling. And although MAS rotation can average out part of it, it is still to strong to be eliminated without further adjustments. wPMLG (windowed phase modulated Lee-Goldburg) is an experiment used to obtain proton spectra with higher resolution. It differentiates itself from one pulse, by the application, during measurement, of a series of pulses in sequence, which allow to drastically reduce the homonuclear coupling: CRAMPS (combined rotation and multiple pulse spectroscopy). This results in much more resolved spectra, which present thinner peaks and a better overall resolution, i.e. by highlighting peaks that are not visible in one pulse spectra.Geppi The pulse sequence is depicted in Fig.3.5

Cross Polarization

The cross polarization (CP) method is at the core of the functioning of solid state NMR: as it brings a great enhancement of the sensitivity of the instrument when characterizing diluted nuclei such as ^{13}C. This is achieved by the transfer of magnetization to the nuclei of interest, from rich nuclei such as ^{1}H. To better understand how this is possible, it is useful to separate the CP experiment in 3 main steps, also depicted in Fig.3.6:

1. A 90° pulse is applied to the proton, with a certain power given by the PLW1 parameter, as it happens for the one pulse experiment;

2. Now the magnetization needs to be transferred to the carbon. This happens **only** if the Hartman-Hahn (Ha-Ha) condition is satisfied, meaning that the polarization

frequencies (or nutation frequencies) of both nuclei have to be equal, as described by the equation 3.1

$$\gamma_I B_{1I} = \gamma_S B_{1S} \tag{3.1}$$

To achieve this, the nuclei should be in close proximity to each other, for a defined time P15, or *contact time*

3. Finally, to acquire the carbon spectra, a decoupling frequency should be applied to the sample.

The decoupling sequence is called SPINAL 64. SPINAL stands for SPin-locking in the Presence of a Nutation Angle Line-narrowing and is one of the most efficient and widely used heteronuclear decoupling sequences in ss-NMR. Its final outcome is a strong reduction of the noise in the signal, which would be present otherwise, due to the strong heteronuclear coupling. Another advantage given by CP is that the delay between scans, or recycle delay (D_1) is based on the relaxation time of the proton, which is much shorter that the ^{13}C one, as will be discussed in the next paragraphs. This makes the acquisition of carbon spectra very quick, even compared to solution NMR. To achieve a good outcome of CP, it is important to optimize the power level of the pulses applied to each nuclei. But it is also crucial to find a good contact time P15, which greatly influences the quality of the signal. This stage of the research has been crucial to achieve a successful outcome of this work, since an important objective consisted in the optimization of ss-NMR experiments on perovskites in order to ensure their quality and reproducibility.

Hahn Echo

This experiment can be used to directly measure the spectra of nuclei with a 1/2 spin, which are not too rare to require a CP. Here the nucleus of interest is directly subjected to a 90° pulse, and after a first period of τ, another pulse at 180° is applied. This second pulse, flips the magnetization on the opposite plane, which causes an echo in the FID response of the sample, that peaks at a duration of τ_2 after the end of the 180° pulse. Basically, the second pulse given to the nuclei is able to reverse the phase evolution of the magnetization and recover the initial one, creating an echo when the spin magnetization is refocused. The pulse scheme is described below in Fig.3.7. Because the nuclei that give signals through this experiments usually have very large ranges of chemical shift,

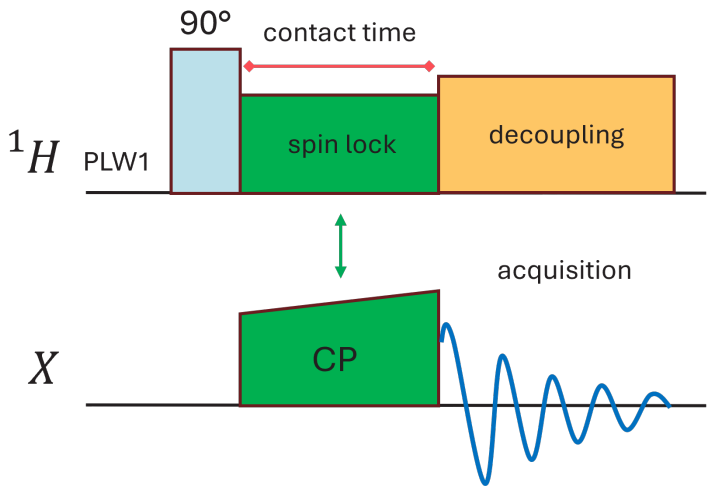

Figure 3.6: Cross polarization pulse sequence: the power of the initial pulse on the proton is set as PLW1; the contact time shows the time needed to transfer the pulse; the decoupling sequence is applied to the proton while acquiring the carbon spectr

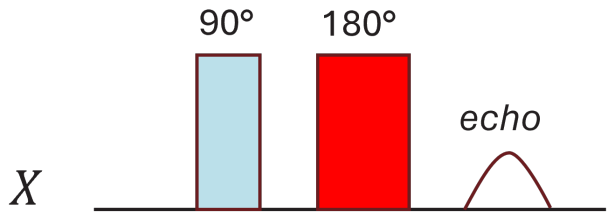

Figure 3.7: Hahn Echo pulse sequence: the two pulses are given to the sample, which then generates an echo that is acquired by the system.

one important parameter to consider is the *Transmitter Frequency Offset* (O1P). O1P describes the center of the frequency range being acquired in the experiment, which is different for every isotope.[36] A frequency offset that is too large, usually does not cause big problems. While when it's to small, there is the risk that the signal falls just outside the range, causing a low signal to noise ratio. After choosing the value of the needed parameters, that can usually be found in literature, the next step is to optimise it to allow a better quality of the signal.

3.3.2.1 Relaxations

Relaxation measurements are fundamental to understand the dynamics of a sample, and in the case of perovskites, are often used to study the local motions of the A-site cation. The basic theory behind this experiments is that, after the nuclei have been subjected to an RF pulse, they become oriented on an axis different from z, then they tend to relax back to equilibrium. This phenomenon is called *longitudinal relaxation* when the pulses

relax back on the z-axis. The magnetization decays exponentially with a time constant T_1. The aim of dynamics experiments is, indeed, to measure these relaxation decays. There are a number of experiments that can be performed on a perovskite sample, which can provide different types of information depending on the time scale of motion of the compounds involved. Below are described the most relevant ones for this specific work.[37]

Inversion recovery

During the production of this work, the Inversion recovery experiment was mainly applied on protons. Here, the sample is subjected to a 180° pulse, which completely flips the magnetization on the opposite plane. When the magnetization vectors are going back to equilibrium, and after a certain period of time τ, which is decided by the executor and is usually called a *vd list*, the measuring pulse is applied. In this case is a 90° pulse. If the relaxation delay is too short, no signal can be seen, therefore it is important to set it correctly. After the acquisition, the relaxation decay for each peak in the proton spectra is fitted to an exponential curve. The scheme of the pulse is depicted in Fig3.8. The downside of this experiment is that the recycle delay D_1 needs to be longer than the longest T_1 of the slowest relaxing spins of the sample, to allow for complete restoration of the magnetization, which usually means that $D_1 > 5 * T_1$. This makes the duration of the experiments quite long. Moreover, only the relaxation times relative to rich nuclei such as ^{1}H can be acquired by Inversion recovery. T_1 is recorded in the order of micro-seconds to pico-seconds, meaning that it can describe very fast movements such as methyl groups' rotations.[38]

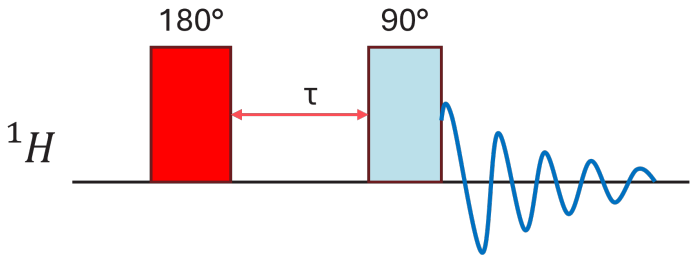

Figure 3.8: Inversion recovery pulse sequence: the 180° pulse is applied to sample to flip the magnetization, after the timeτ the measuing pulse is applied

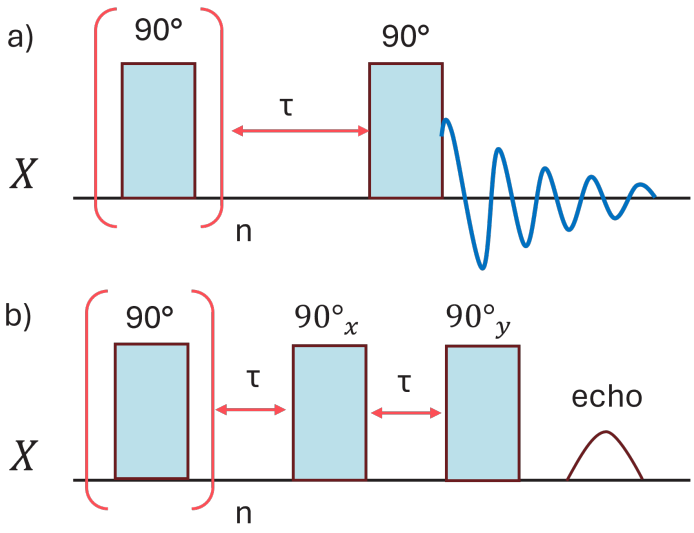

Figure 3.9: a)Saturation recovery pulse sequence: a series of n pulses of 90° are given to the sample to saturate the magnetization; after a time τ, the final pulse is applied and acquisition starts; b) saturation recovery echo pulse sequence. A solid echo pulse sequence is applied after the first pulse, the relaxation time is recorded for the echo.

Saturation recovery

Saturation recovery's principle is very similar to inversion recovery, with the important difference that initially, a sequence of 90° pulses are applied to the sample, instead of a single 180° one. Here, the transitions are *saturated* and no signal can be detected. Then relaxation occurs and a final 90° readout pulse is applied. This allows for quicker measurements, since there is no need to wait for complete relaxation of the nuclei. Fig.3.9 describes the pulse sequence. A modification to the experiment can be applied: to achieve an even better resolution of the signal, 90° pulse is sent instead of a 180° pulse, with the aim to achieve the refocusing of spin magnetization. For this work, this experiment was mainly applied on Tin, which has a very short T_1. However, due to the low signal strength, numerous scans were required. The main aim of this experiment was to set the Sn T_1 which is mainly useful to derive the recycle delay, that is, in turn, set for other sets of experiments such as Hahn Echo.

TORCHIA

As previously mentioned, inversion recovery does not allow for the fitting of T_1 on diluted nuclei, since their magnetization is not strong enough. For this aim, the pulse sequence TORCHIA, depicted in Fig.3.10 is used. This experiment exploits the set up of CP pulses

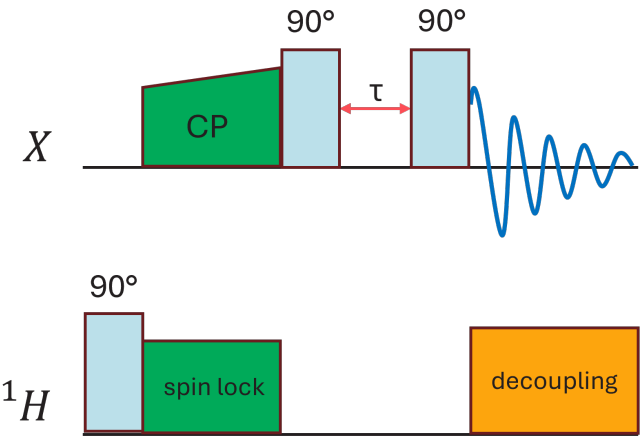

Figure 3.10: TORCHIA pulse sequence: the CP pulse scheme is exploited, but instead of direct acquisition, the time τ is recorded right after the spin lock and before the decoupling

to achieve the relaxation time of ^{13}C. After the spin lock between the nuclei has occurred and magnetization has been transferred between ^{1}H and ^{13}C, a 90° pulse is applied on the observed nucleus, the time τ is set, and the final measuring pulse is sent. Here, the main advantage is that there is no need to wait for full recovery of the magnetization, and the recycle delay between the scans is the one need by protons to relax, therefore the time needed for this experiment to be performed, it is quite shorter compared to inversion recovery. Moreover, since protons relax faster than ^{13}C, D_1 should only be set to be 3 times higher than T_1. TORCHIA is mainly used to highlight the dynamics of aliphatic and aromatic groups, such as eventual benzene ring flips.[38], [39]

Spin lattice orientation time in the rotating frame

This experiments exploit the pulse sequence of CP, as does TORCHIA, but the measurements are referred to the rotating frame. In fact, the spin lattice relaxation in the rotating frame describes the return to equilibrium of transverse magnetization (on the xy plane) in the presence of spin locking, i.e. during a CP experiment. Therefore, the applied pulses act on the rotor axis, which is relative to the magic angle, and not to the lab reference system. This is why the T_1 measured here are called $T_{1\rho}$. This kinds of experiments give important information on the mobility of the organic chains, since the relaxation times lie in the order of milli to micro-seconds. Likewise to the TORCHIA experiment, the pulse program is the one used for CP. In fact the $T_{1\rho}$ experiments are relative to the heteronucleus spectra, but they are able to measure the relaxation times of both proton $T_{1\rho H}$ and the heteronucleus $T_{1\rho X}$, which in this case, is ^{13}C, depending

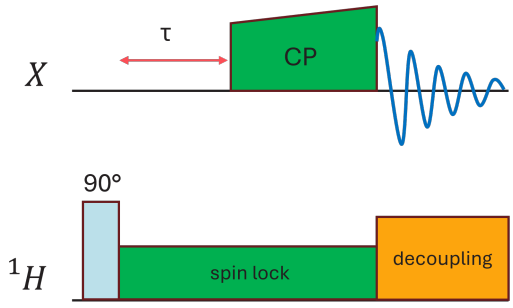

(a) depiction of the pulse sequence for the fitting of $T_{1\rho H}$: the time τ is recorded during the spin lock phase to achieve the $T_{1\rho}$ of the proton, before magnetization is transferred to the carbon

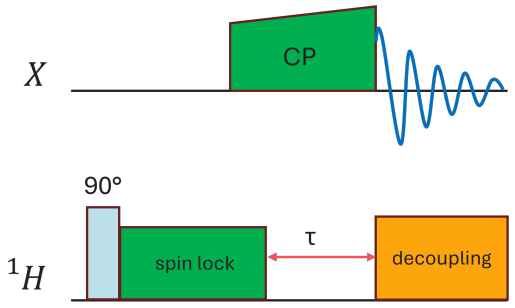

(b) depiction of the pulse sequence for the fitting of $T_{1\rho C}$: after the magnetization has been transferred, the time τ is set so that the carbon nuclei $T_{1\rho}$ can be fitted in an exponential decay curve.

on where τ is recorded: either before or after the spin-lock has taken place. These experiments are vital for a better understanding of the mobility of the A-site cations, since they can give information about the phenyl ring movements and the orientation of the sidechains [39]. For this purpose, the results of these analysis carried out on two different samples of PEA_2SnI_4 will be compared in the next chapter, with the aim of highlighting the difference that can be brought by the use of two distinct precursors in the synthesis of the same perovskite.

3.4 Characterization: Crystal XRD

Single-crystal X-ray diffraction experiments were performed on a Bruker Apex II diffractometer, equipped with a CMOS detector, by using Mo Kα radiation. The analyses were carried out at room temperature (298K). The crystallographic structure of the PEA_2SnI_4 perovskite was reported using the visualization for electronic and structural analysis (VESTA) program.

The three samples of the synthesised perovskites were subjected to an analysis of the unit cell, which is determined according to the data acquired by the analysis, such as bond lengths and angles. Subsequently, the complete crystalline structures of only the two PEA_2SnI_4 samples were determined.

Results and discussion

4.1 Tin Iodide

Because the main problem regarding tin-based perovskites is relative to their degradation after exposition to air, it is crucial to have an idea of what the degradation products could look like. For this reason, ss-NMR characterization was carried out on Tin Iodide SnI_2 with the aim of deriving the chemical shift of this compound and the shape of its spectra. Tin Iodide was characterized using Hahn Echo at different MAS speeds and different recycle delays D_1. The best results were achieved at a MAS speed of 42kHz, as lower speeds led to the detection of spinning side-bands. The optimal value of D_1 is usually obtained starting from the results of the relaxation measurements, in this case the preferred one would be saturation recovery. However, to achieve good quality saturation recovery, it is important to already have the right frequency offset, which is determined by conducting the Hahn Echo experiment. Therefore, Hahn Echo experiments are typically carried out prior to saturation recovery. Therefore, the same experiment at the same MAS speed was performed three times, with different arbitrary values of D_1. In Fig.4.1 are reported three spectra of the same sample, spinning at 42kHz with different recycle delays (0,001. 1 and 3s). It is interesting to notice that with increasing D_1 from 0,01s to 1 s, the number of peak increases from 1 to 2, with the first peak being slightly shifted to the right. By increasing again the D_1 to 3s the resolution becomes much higher and the two peaks are much more defined. At the same time, the intensity of the signal raises seemingly. It is known and reported in literature, that solid SnI_2 presents two different crystal structures: α and β. Where α has a monoclinic unit cell, and presents a layered structure where 2/3 of the tin atoms are involved in a capped trigonal prismatic coordination with 5 halides, while the rest presents an octahedral coordination with 6 iodines. [40] Fig.4.2 shows the

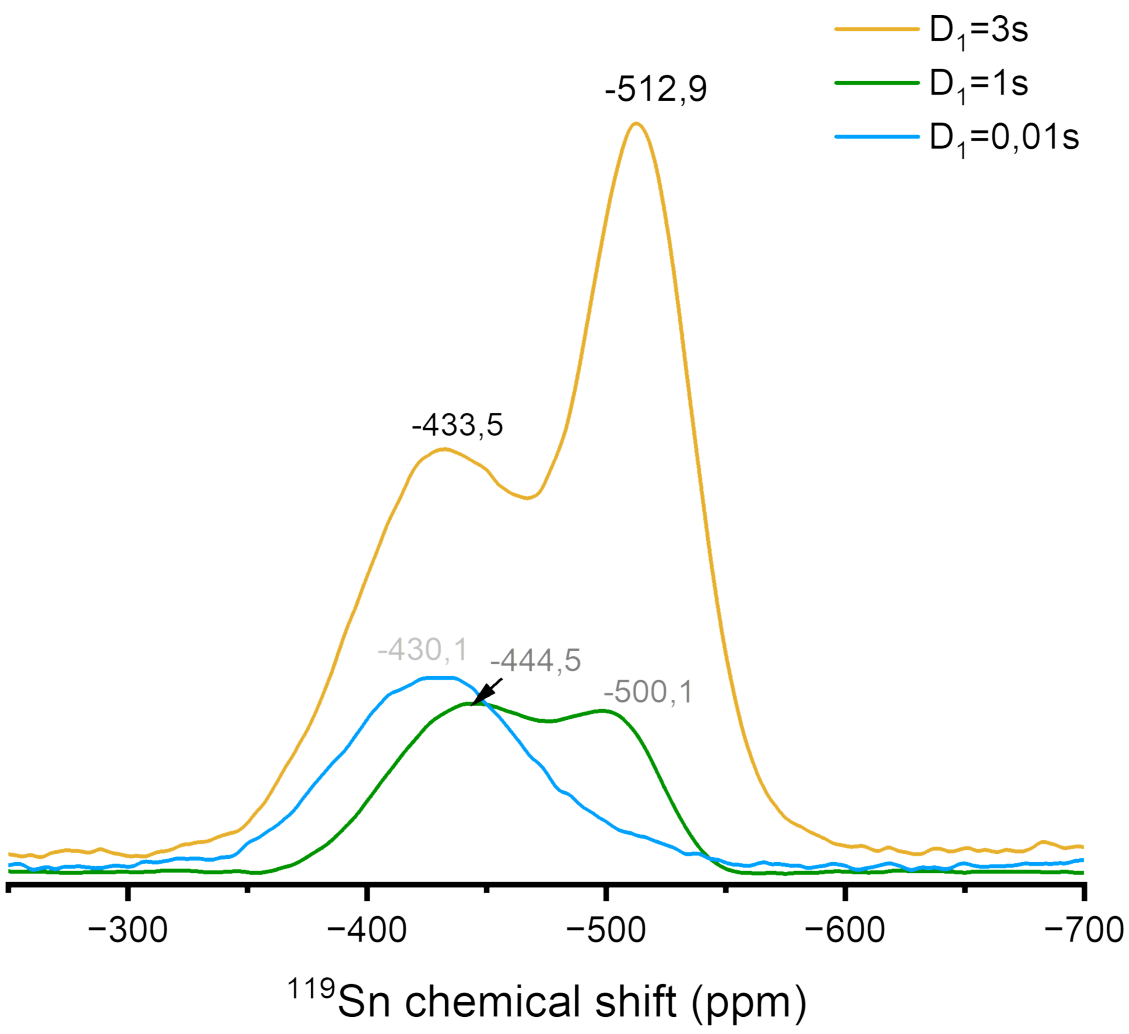

Figure 4.1: Comparison of the 3 ^{119}Sn signal recorded at different D_1

crystalline structure of the α phase of SnI_2. Because the α phase the most stable at room temperature, this is the one taken in consideration for NMR analysis. Indeed, the peaks shown in the spectrum indicate the two coordination environments of ^{119}Sn. The second peak, which emerges only at longer recycle delays, is likely associated with the octahedral tin, as its more ordered structure leads to slower relaxation.

These results clearly prove the precision and sensitivity of solid state NMR experiments, giving a demonstration on how different parameters can affect the resolution of the spectra and therefore highlighting the importance of their optimization. Additionally, it is evident that solid-state NMR is a complex instrument that demands a deep understanding of both its experimental settings and underlying operating principles. The acquisition of the SnI_2

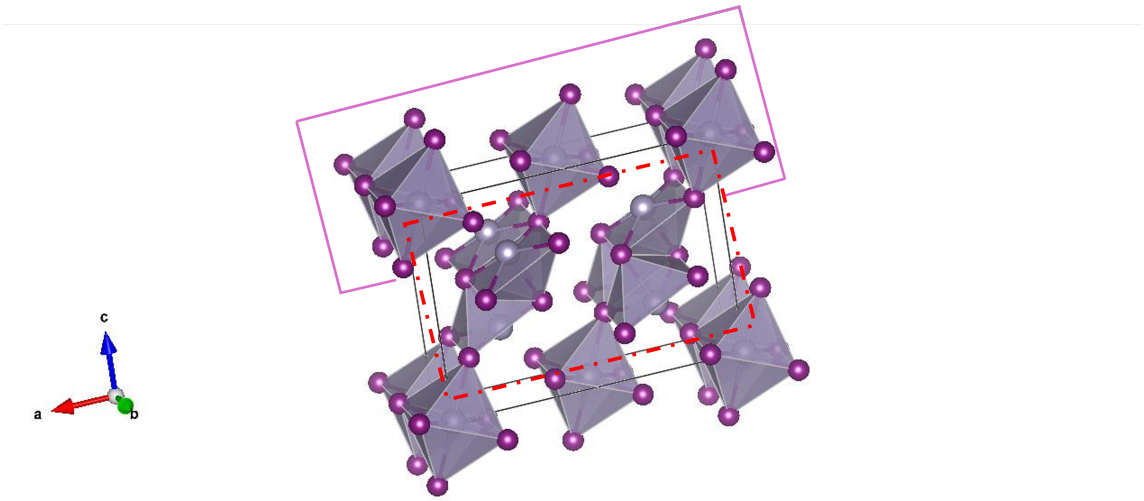

Figure 4.2: Depiction of the two coordination phases of SnI_2, obtained through VESTA. Where the purple highlighted one sees Sn^{2+} coordinated 6 times to I^- while the red highlighted one relates to 5-fold coordinated Sn

spectra allows for a more precise identification of the compound's potential presence in tin-based perovskites, which could be due to incomplete reactions containing perovskite precursors or to the initiation of a degradation process. The experiments conducted on this compound were highly valuable in developing the research for this work, as they offered deeper insights into the experimental procedures and contributed to a more comprehensive understanding of the study's overall development.

4.2 Formamidinium Tin Iodide

Formamidinium tin iodide ($FASnI_3$) is a 3D hybrid perovskite with cubic unit cell. Meaning that the formamidnium molecules are positioned inside the octahedral cavities formed by the inorganic cells, and they interact with the iodine anions. XRD analysis of the unit cell was carried out on the syntheisised perovskite to make sure that it matched with literature data. The unit cell parameters, indeed, matched with the data found by Khaman et. al[34] and the structure of the unit cell was confirmed, the values are reported in In Tab.4.1. In Fig.4.3 the image of the cubic perovskite is reported, where the formamidinium groups can be clearly distinguished in the interstitial cavities of the structure. The characterization of this compound through ss-NMR was delineated by

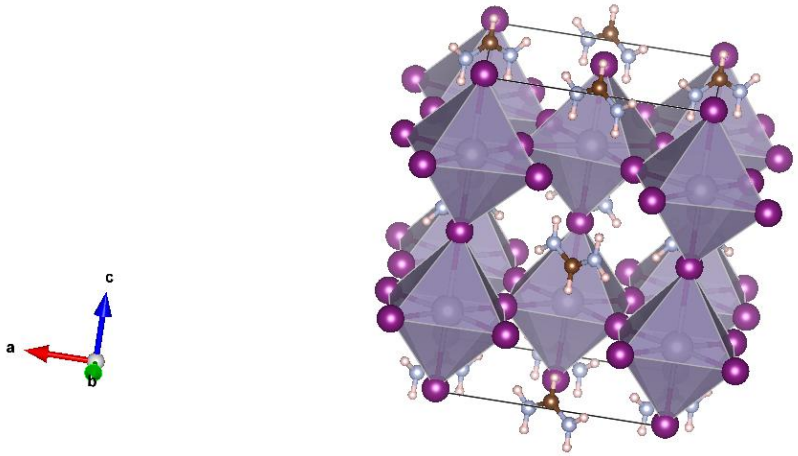

Figure 4.3: Unit cell of $FASnI_3$ [34].

compound	$FASnI_3$
unit cell	cubic
a	8.83790Å
b	8.83790Å
c	12.40660Å
α	90°
β	90°
γ	90°

Table 4.1: unit cell prameters of the FASnI3 unit cell from [34]

quite a few problems. First and foremost, the formamidinium molecule is highly mobile, indicating that the carbons of formamidinium spin rapidly inside the perovskite's

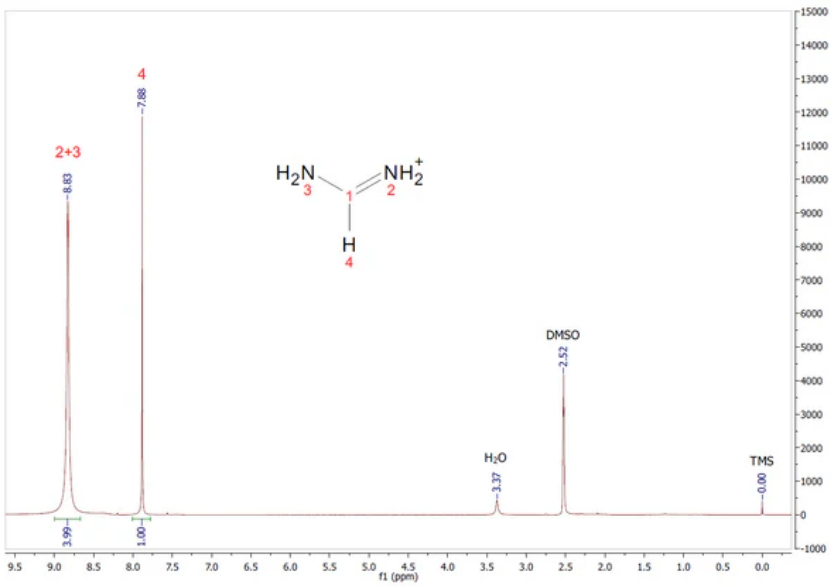

Figure 4.4: ^{1}H spectrum in solution NMR of FAI by Solaveni

cavities. For this reason is almost impossible to obtain a ^{13}C spectra with the probe at disposal. Cross Polarization is highly influenced by the mobility of the atoms, since, to achieve the Hartman-Hahn condition, local proximity for a determined period of time is required. Therefore, if the nuclei are too far apart or if they spin too fast, the CP will be negatively affected, because the magnetization transfer from proton to the heteronuclei will be hampered. This problem could be overcome by lowering the temperature at 100K to minimize molecular motion, but it was not possible with the current setup.

The ^{1}H spectra were acquired through direct excitation (One Pulse experiment). However, this pulse sequence is not characterised by great resolution, since it is influenced by the strong homonuclear dipolar coupling between protons with consequent loss of resolution. A better resolution can be achieved at high MAS spinning rates, because this helps with reducing a great fraction of the homonuclear coupling contributions. This produces thinner an more intense lines on the spectra. To have a better idea of where the ^{1}H signal would fall, a spectrum of the perovskite precursor FAI by Solaveni, is reported in Fig.4.4. In Fig.4.5 the ^{1}H spectra of $FASnI_3$ is depicted. As depicted in 4.4, 2 peaks should be present in the final spectra, one related to the ammidinic group and one for the ^{1}H directly bonded to the carbon. The peak obtained by One Pulse is larger compare to the prediction, but its value is coherent with the proton on position 4, and the small "shoulder" on the left can be traced to the peaks of the ammidinic groups.

Finally, in theory, it would be possible to acquire a ^{119}Sn spectrum of $FASnI_3$ by Hahn echo.

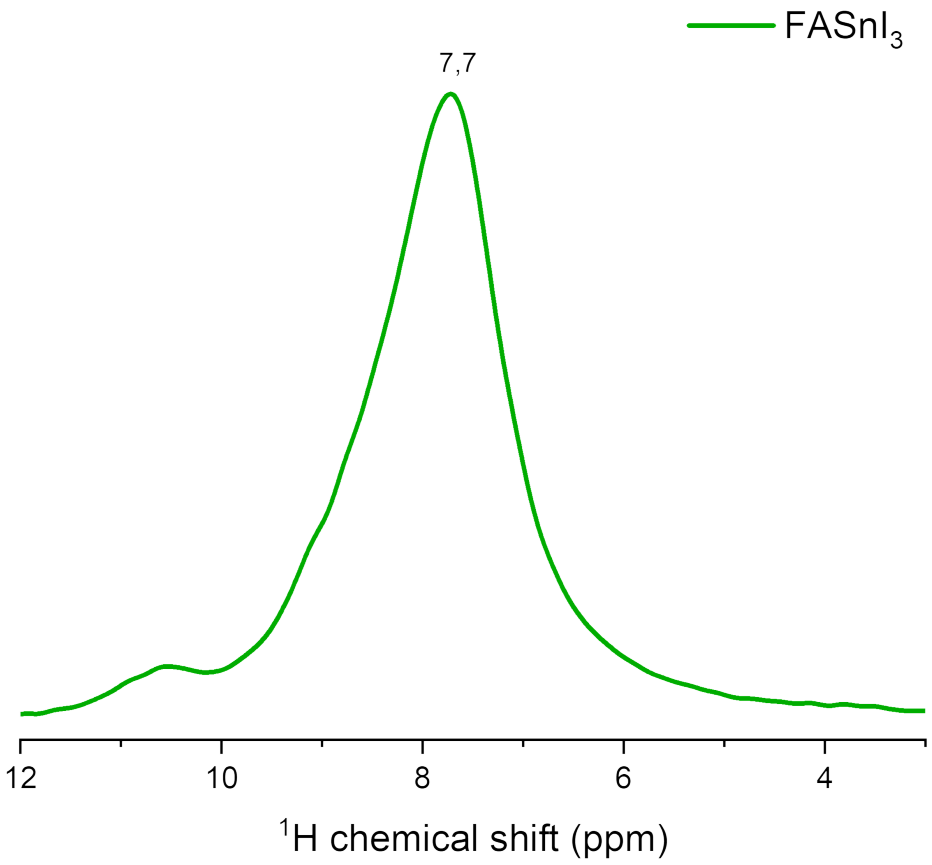

Figure 4.5: One Pulse on $FASnI_3$ with MASR=42kHz at T=278K

Nevertheless, the packed samples of the perovskite, demonstrated a peculiar behaviour when they were spun at high MAS speed. In fact, we observed a recrystallization of the FASnI3 powders during high spin rates, forming crystalline pellets unevenly distributed inside the rotor (Fig.4.6) that would compromise its spinning stability, thus causing the rotor to stop. Several tries were carried out on $FASnI_3$samples prepared starting from different precursors (SnO and SnI_2), the same behaviour was always observed. 3D perovskites are known to have have a marked self healing behaviour; thus the high pressure induced by the fast rotation, jointly with the frictional heating acting from the surface, could trigger a recrystallization phenomenon of the powder[41]. This hypothesis is still under investigation. For this reason, it was not possible to perform further experiments on this material in the framework of this work. The reason behind this peculiar behaviour is still not certain.

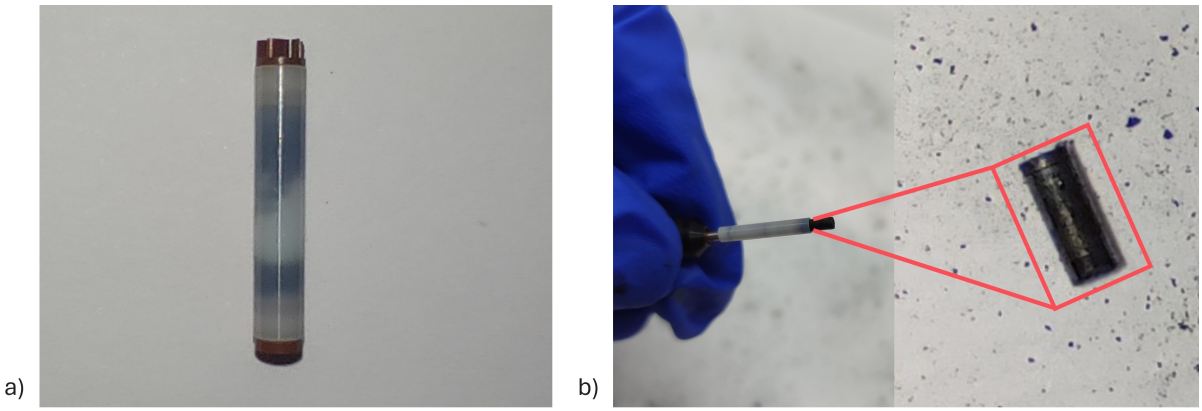

Figure 4.6: a) picture of the rotor after MAS failure; b) picture of the pellet inside the rotor and outside

4.3 Phenethylammonium Tin Iodide

The primary purpose of this study is to characterize the 2D perovskite PEA_2SnI_4. Specifically, this work seeks to examine the differences in its crystalline structure when synthesized from two distinct precursors: tin oxide (SnO) and tin iodide (SnI_2). At the time of writing, there are very few reports on ss-NMR of tin perovskites, and none of them on layered tin perovskites.[28] Hence, before performing complex analysis, it is required to implement simpler experiments that, nevertheless, allow an exhaustive comprehension of the perovskite's structure and general features. At the same time, it is important to have a general idea of what the structure of perovskite looks like. For this purpose, crystal XRD was employed on both the interested perovskites. From this point on, to distinguish between the two materials, PEA_2SnI_4 from SnO will be called PEA_1, while the perovskite based on SnI_2 will be referred to as PEA_2. The data found in literature regarding XRD on PEA_2SnI_4 describe the unit cell as monoclinic, the unit cell parameters found by Zhang et.al[42], and consequently relaxed by Folpini et al.[43] are reported in Table 4.2. Other studies on the PEA_2SnI_4 structure highlight that the organic layer presents some structural disorder in over two positions, as well as the inorganic longitudinal iodines[14]. Thus, a certain degree of mobility of the organic cations is expected. In Fig.4.7 the XRD structure found in literature is reported as a reference. The single crystal-XRD analysis performed for this study on both PEA_2SnI_4 perovskites showed consistency with the data available in the literature; however, small differences were observed between the two. In Fig.4.8 the two structure presenting only the inorganic frame are reported, while the unit

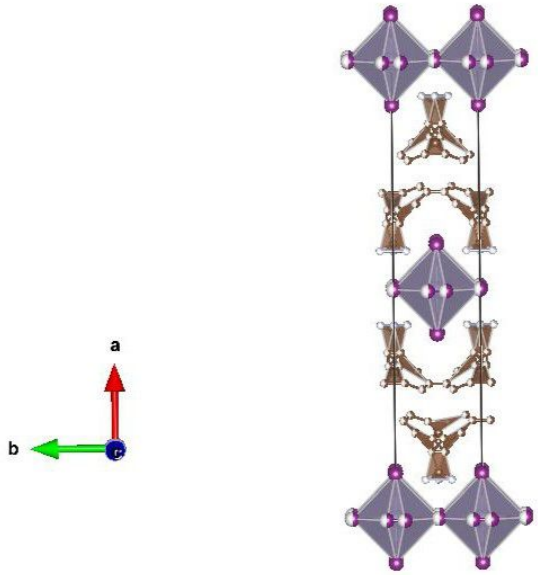

Figure 4.7: The perovskitic structure is observed from all the reference axis. It shows the structural disorder in bot the organic and inorganic layer

cell parameters of the three cells are described in 4.2 Some significant observations have emerged. The parameters determined for the two cells do not exactly align with existing literature: the unit cell and spacial group reported are the same (monoclinic, C 2/m), but two of the lengths of the unit cell were found to be double those reported in the references. This discrepancy arises because the inorganic layers are not uniform; In fact, by looking at the structure reported, it is possible to see that in the PEA_1 structure, 2 of the 3 layers show a disorder in the longitudinal iodines. While only one layer of PEA_2 reports the same disorder. The organic cations appear to be highly disorderd in our structures at room temperature, and it was not possible to identify their positions in the unit cell. For this reason, only the structure of the inorganic motif is shown in figure4.8

Overall, the two structures are very similar to each other, but they present a different degree of disorder. This variations raise new questions about whether the selection of precursors used in synthesizing the perovskite could impact the material's final structure and, consequently, its properties. To explore these structural discrepancies further and determine their relevance, the two perovskites were characterized using solid-state NMR.

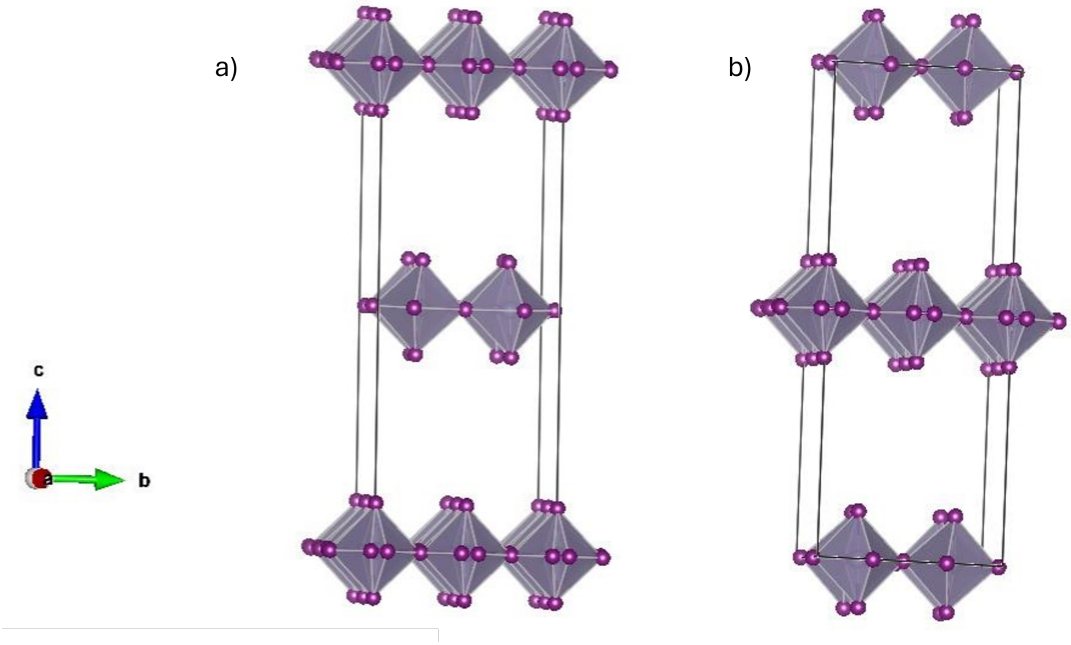

Figure 4.8: a) structure of PEA_1 acquired by XRD b) structure of PEA_2 acquired by XRD

Compound	PEA_2SnI_4 reference	PEA_1	PEA_2
unit cell	monoclinic	monoclinic	monoclinic
spacial group	C 2/m	C 2/m	C 2/m
a	32.29900Å	12.33190	12.35000
b	6.10420Å	12.26020	12.26600
c	6.13780Å	32.93350	32.94000
α	90°	90°	90°
β	93.9610°	97.5770°	97.7000°
γ	90°	90°	90°

Table 4.2: Comparison of the unit cell parameters of PEA_2SnI_4 from [43] and our samples.

4.3.1 SS-NMR

Since PEA_2SnI_4 is a hybrid perovskite, it is good practice to start the characterization from the organic layer. This is because a comparison between the obtained spectra and eventual literature data is much more likely to be achieved when characterizing an organic compound such as phenethylammonium. Indeed, to have an idea of where the peaks of the compound would fall, two predictions on the phenethylammonium molecule based on solution NMR were carried out through ChemDraw on both ^{1}H and ^{13}C, which are reported in Fig.4.9.

^{1}H characterization: One Pulse and wpmlg

The initial experiments conducted included CP on ^{13}C as well as both one-pulse and wpmlg on ^{1}H. Starting from ^{1}H characterization, below are reported the comparative spectra of One pulse 4.10a and of wpmlg4.10b on the two perovskites. As shown in Fig.4.10a, the one-pulse spectrum reveals only two peaks for each compound. This is attributed to the strong homonuclear dipolar coupling of protons, even when magic angle (MA) spinning is performed at the maximum speed of 42kHz. It is interesting to notice a slight shift between the two compounds, related to the lower peak of the one pulse. To achieve better-resolved spectra, and confirm the shift between the two peaks that appeared in the One Pulse spectra, the wpmlg pulse sequence can be employed. Although this technique cannot completely average out all contributions from homonuclear coupling, it does enhance both the intensity and resolution of the peaks. Observing Fig4.10b, the difference between the two techniques becomes evident, as the two peaks from each compound, are much better defined and the lines become narrower.The peaks obtained from these experiments align well with the predicted values, allowing clear differentiation between the two types of 1H present in the organic molecule: the aromatic and the aliphatic ones. However, a clear shift between the two lower peaks of PEA_1 and PEA_2 can be observed. This suggests a different spatial order of the cations in the two compounds particularly related to the position of the etylammonium linkers that interact electrostatically with the perovskite inorganic sheets.

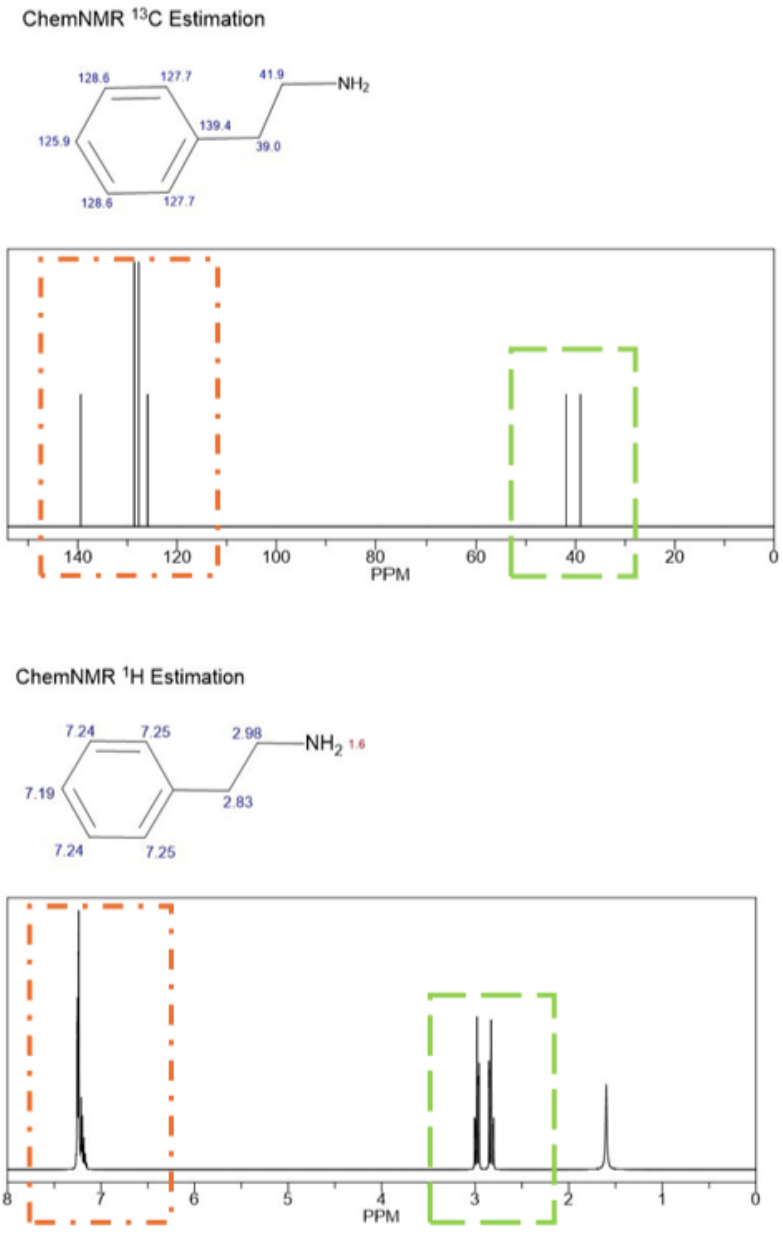

Figure 4.9: Prediction of the NMR spectra of phenethylammine, where the orange highlighted regions correspond to the aromatic nuclei, while the green highlighted ones are the aliphatic nuclei. Each atom has its corresponding value in ppm written beside.

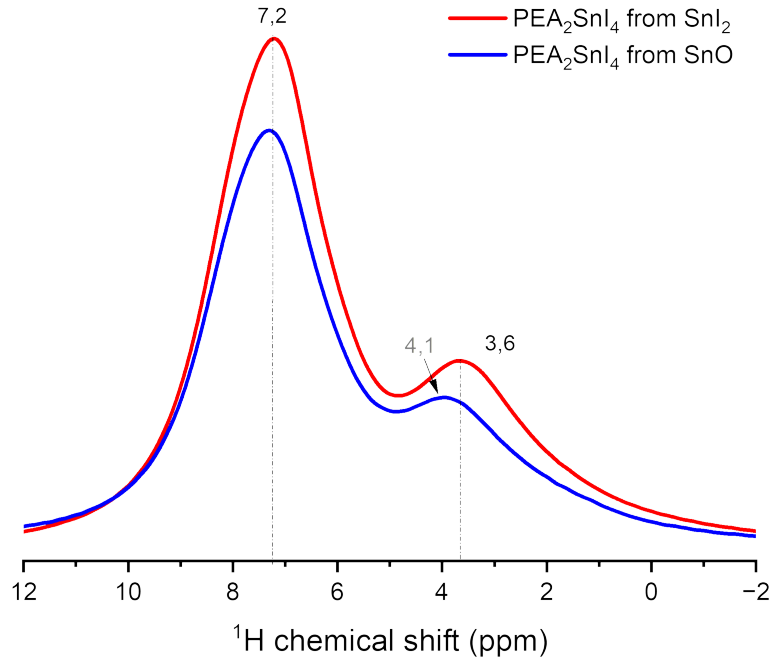

(a) One Pulse experiment on ^{1}H at MASR=42kHz: comparison between $PEA_1$and PEA_2

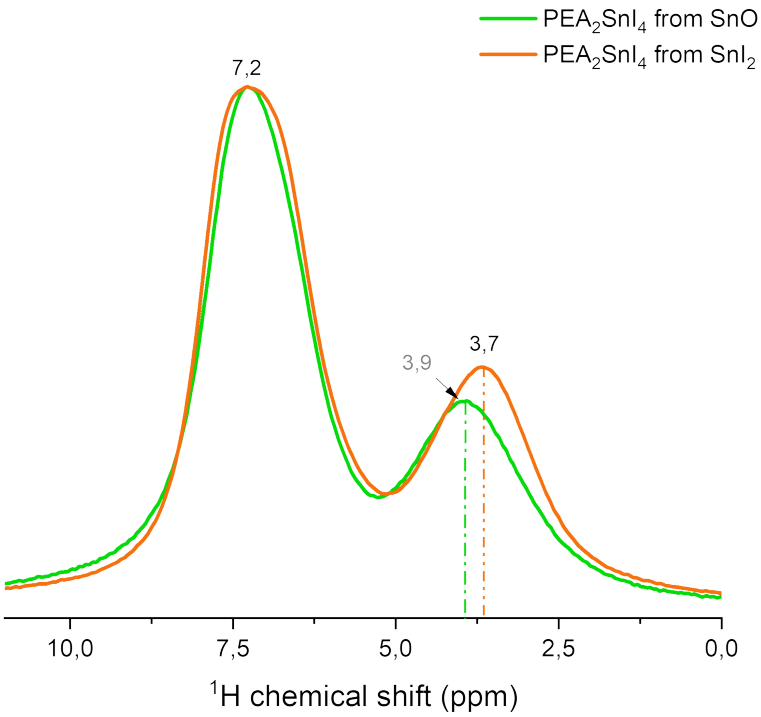

(b) wpmlg experiment on ^{1}H at MASR=17kHz: comparison between $PEA_1$and PEA_2

Figure 4.10

Cross Polarization on ^{13}C

The results of CP on ^{13}C, reported in Fig.4.11 are also consistent with the predicted spectra: three peaks are displayed in the aromatic region, as opposed to four, and two in the aliphatic region. CP is quite effective in resolving spectra of diluted nuclei, like carbon-13. However, it's crucial to remember that while ss-NMR shares the same fundamental principles as solution NMR, there are significant differences between the two. And these distinctions arise precisely from the fact that the sample is fixed in a solid state rather than freely moving in a solution, which leads to variations in couplings, and therefore results in different-looking signals. Nevertheless, the acquisition of ^{13}C spectra by CP results in great quality spectra, and a very quick time of acquisition. It was found that the best MAS rate for these pulse sequence is at 15kHz, due to the fact that heteronuclear decoupling is negatively influenced by the speed of the MAS.

In any case, comparing the spectra of the two compounds, no obvious discrepancy is observed, neither in the number of peaks, nor in the chemical shift. The two organic molecule correspond and can be addressed as phelethylammonium. In order to asses the correlation between the ^{1}H and ^{13}C nuclei, an interesting 2D experiment can be conducted, called indeed HETCOR, or heteronuclei correlation. HETCOR is able to associate the signals of the protons to their corresponding carbons. Below are reported two HETCOR measured on PEA_1. They are both recorded at the same MAS speed of 15kHz, but with different contact times (P15), which determine the resolution of the output signal. In fact, it is interesting to notice how, when using short times, only the first neighbours are recorded, meaning the protons that are directly bonded to the respective carbon, as shown in Fig.4.12 While, when increasing P15 to ten times as the previous, as depicted in Fig4.13, it is possible to notice the relations of each ^{1}H to each ^{13}C of the spectrum.

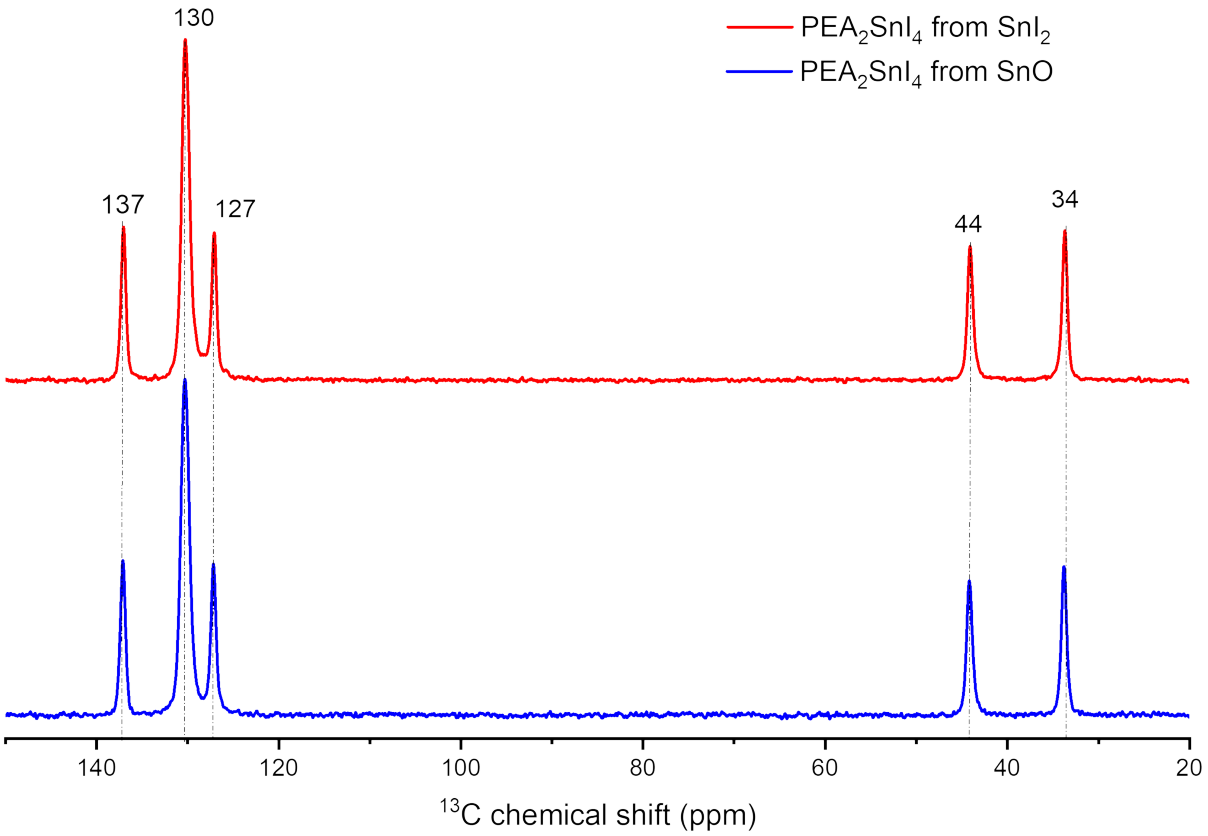

Figure 4.11: CP spectra on ^{13}C with MASR=15kHz and T=298K

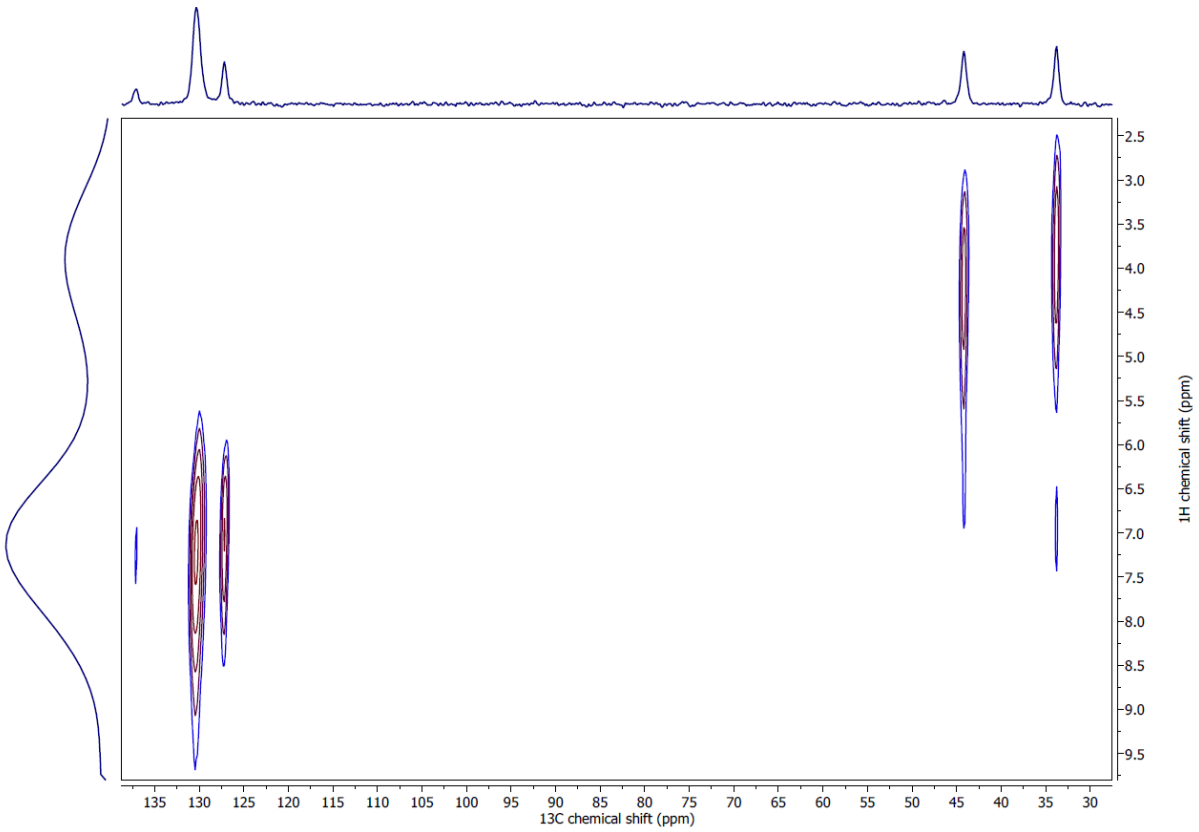

Figure 4.12: HETCOR on PEA_2SnI_4 with MARSR=15kHz and p15=200µs

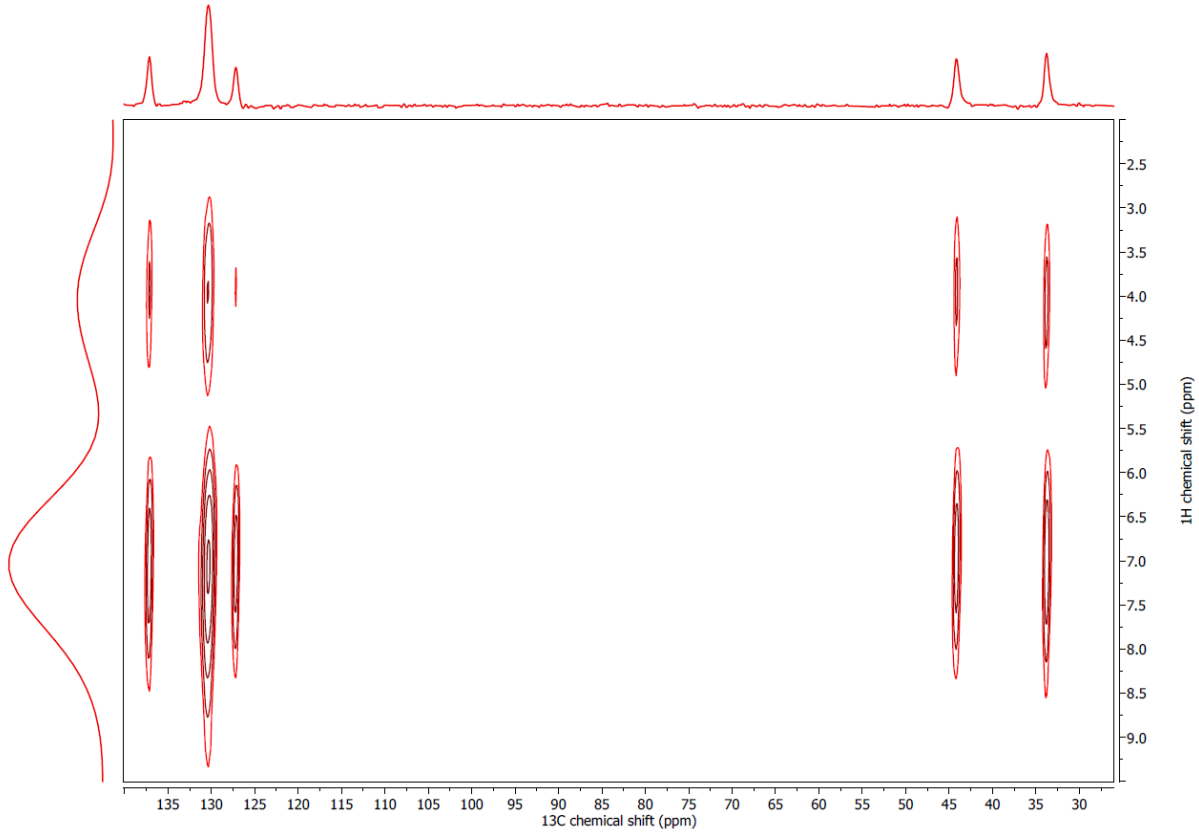

Figure 4.13: HETCOR on PEA_2SnI_4 with MARSR=15kHz and p15=2000µs

Characterization of ^{119}Sn

After confirming that the spectra obtained through ss-NMR aligned with the predicted results, the next step consists in analyzing ^{119}Sn. Tin ss-NMR spectra had not been investigated before in this particular perovskite. To achieve a spectrum on this nucleus, two methods were considered: cross-polarization (CP) $^{1}/^{119}$Sn and direct irradiation using the Hahn echo technique. Both experiments were performed on the sample, and it was expected that the outcomes would be identical, as theoretically, the transfer of magnetization to ^{119}Sn via ^{1}H in the CP method should not influence the position of the resulting signal.

CP on ^{119}Sn

The parameters of the CP were defined on the basis of other experiments previously performed on tin. Among them, the frequency offset of ^{119}Sn, which is equal to 200ppm. But when performing the analysis on PEA_1, the results showed a spectrum with no signal. This raised questions on the position and dynamics of the organic cations, since CP is strongly influenced by spacial proximity. This could mean that the PEA cation has a different orientation than expected, that brings the protons further form tin. Or, more likely, that it's mobility is much higher than predicted. On the contrary, as shown in Fig.4.14, the same experiment performed on PEA_2 generates a signal in the O1P that was expected. These results prove that there is definitely a difference between the two compounds and that it is likely be related to the different mobility of the organic cations in the lattice.

Hahn Echo

With the objective of investigating further the ^{119}Sn spectrum, the Hahn echo was performed using the same frequency offset as the one chosen for CP, whicle the recycle delay was chosen deliberately and optimised during a number of measurements. The Hahn echo acquisition was successful for both the compounds, and yielded a single-peak spectrum, as depicted in the comparative spectra on Fig.4.15. Nevertheless, the two peaks are shifted by the order of ten ppms, and the peak of PEA_2 results thinner and higher in intensity. This distinction between the two compounds might be given by a slightly different local environment on tin, where the one on PEA_1 results less defined, and likely more disor-

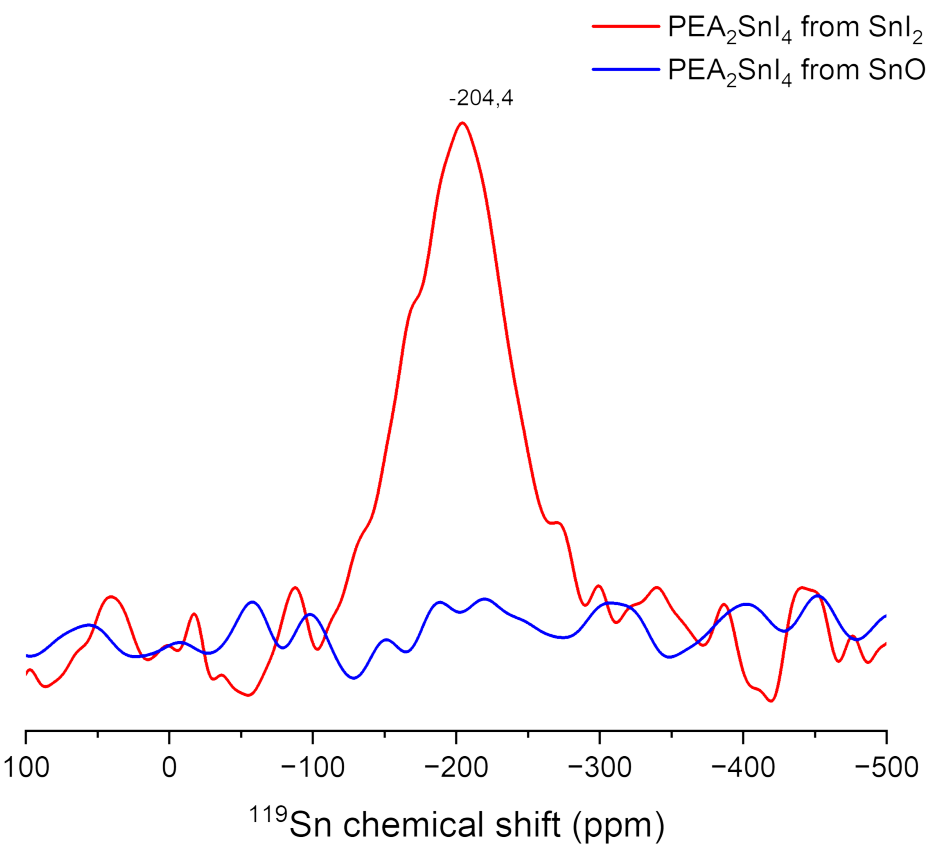

Figure 4.14: CP on ^{119}Sn, performed with MASR=15kHz and T=298K: comparison between PEA_1 and PEA_2

dered that the one on PEA_2.

But even more interestingly, the signals acquired by both Hahn echoes, are also shifted from the CP signal recorded on PEA_2, by $\sim$ 50ppm. A small variation in the chemical shift between the experiments could be expected, since the pulse sequences -and therefore the type of irradiation- are different, but one as large as 50ppm, indicates that the results of the two experiments are dominated by distinct parameters and features of the perovskite. Indeed, as mentioned before, contrarily to the Hahn echo, the CP is highly influenced by the vicinity of the nuclei interacting with each other to generate the signal (in this case ^{1}H and ^{119}Sn), confirming that the absence of the signal on PEA_1 can be caused by a different orientation of the organic cation, or even, as it happens for $FASnI_3$, by higher mobility of the latter. To further exclude a difference in tin nuclei, a saturation recovery echo was carried out for both samples. The saturation recovery analyses, among them, the sat-rec echo serve for the determination of the T_1 on nuclei that can be directly irradiated but have a long relaxation time, or a low intensity signal. The results of this measurement report very short T_1 for both the compounds, with very close values. For PEA_1, $T_1 = 4.89E-4$ while for PEA_2 $T_1 = 5.77E-4$. Such short relaxation times might be due to the interactions of tin with the quadrupolar nuclei of iodine, which can average out the shift in T_1 due to spacial disorder. Therefore, it is important to investigate further the nature of the difference between the two samples in the organic layer of the perovskite.

4.3.1.1 Relaxation measurements

The results obtained until this moment, rose the assumption that the compounds have overall the same long range order of the inorganic layer, but present a difference in the local behaviour. Which sees the organic layer of PEA_1 more disordered compared to the PEA_2 one. This behaviour could also be due to the presence of defects in the perovskite, such as interstitials or passivating agents, that would affect the packing of the organic layer, and therefore increasing its disorder. To further confirm our suspects, the relaxation measurements on carbon and proton are carried out. Because they are influenced by vicinity and mobility of the atoms, they turn out to be extremely useful for this purpose. The movements that can take place between the atoms of the PEA cation, are mainly of three kinds: the reorientation of the aminic group NH_3^+, the rotation around two sites

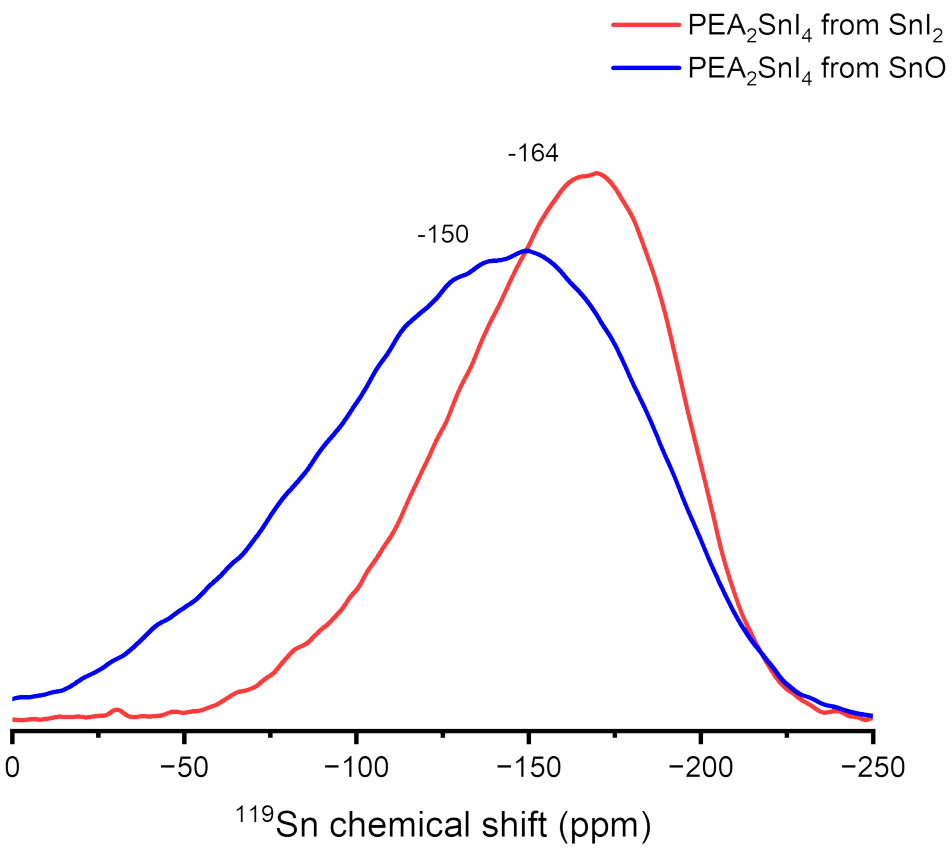

Figure 4.15: Hahn echo on ^{119}Sn, performed with MASR=42kHz and T=298K: comparison between PEA_1 and PEA_2

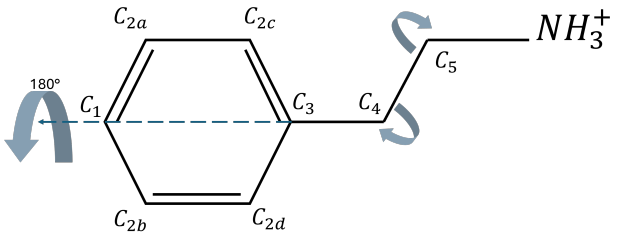

Figure 4.16: Depiction of the molecular movements that can take place in thePEA cation

of the ethyl chain (CH_2CH_2) and the 180° flip of the phenyl ring around its symmetry axis. Among them, the ones that can be investigated in this work include only the carbon containing groups, of which the phenyl ring is the fastest (10^{-6} to 10^{-5}s)[44][29]. These movements are outlined in Fig4.16. TORCHIA experiments are able to give information about slower molecular motions, such as those involving side-chain rotations, typically in the millisecond to second timescale. Hence, it is an important measurement to perform when wanting to compare the mobility of the organic cation on two distinct samples. Moreover, it is able to capture motions that modulate the heteronuclear dipolar couplings, making it more suitable for studying how atoms move relative to one another over longer timescales. In Fig.4.17 is depicted the comparison between the acquisition on both compounds, with a reference ^{13}C spectrum to give a clearer picture of the relaxation times of each peak. This results accurately describe the difference between the T_1, showing that PEA_1 carbons relax much more rapidly compared to the ones on PEA_2. The difference is visible for each carbon atom, but it is even more evident for the aromatic ones, suggesting that the phenyl ring carbons on PEA_1 move faster compared to the ones on PEA_2. Moreover, it is also interesting to observe the error on each signal, as the ones recorded on the carbons of PEA_1, specifically on C_3 are much larger, hinting at a poorer quality of the signal, which can be traced back to a higher degree of disorder. Indeed, since TORCHIA involves cross-polarization, the efficiency of magnetization transfer depends on the rigidity or mobility of the molecular segments, hence, it is more effective in detecting rigid or semi-rigid regions of the molecule. Therefore, it provides insights into motional constraints and order parameters. With the same purpose as TORCHIA, also the spin relaxation experiments in the rotating frame were performed, as depicted in Fig4.18 and 4.19. These measurement are used to record motions that happen with shorter time spans (micro-seconds). Such movements of the atoms are also fundamental to understand the mobility of the cation in the organic layer, specifically, they can pro-

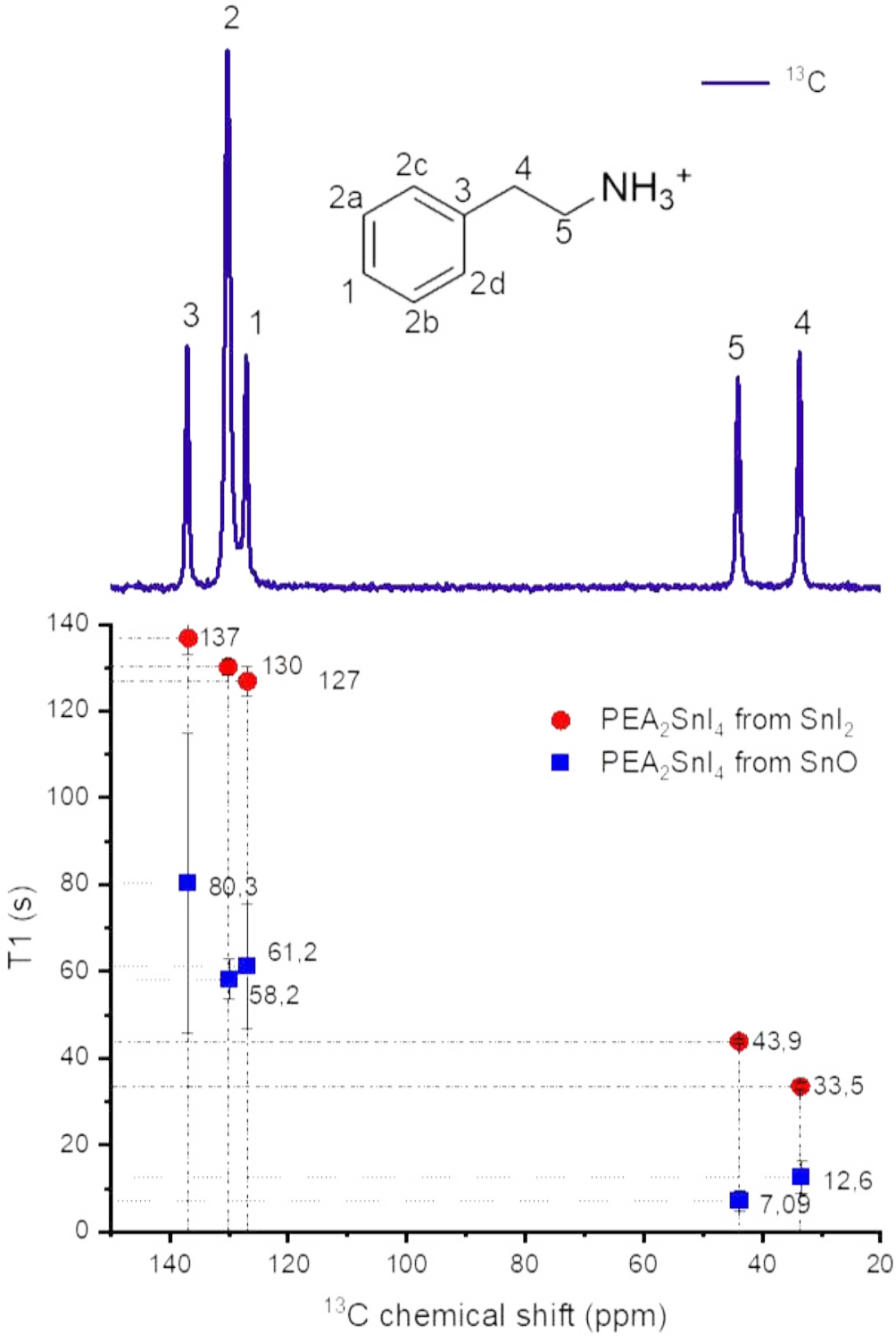

Figure 4.17: T_1 relaxation times obtained from TORCHIA, recorded at MASR=25kHz and T=298K

vide information about the local fluctuations of the molecule, and regarding how much freedom a particular carbon atom has in its own local environment. Also in this case, the relaxation times reported on the atoms of PEA_1 are faster that the ones reported on PEA_2. Specifically, the carbons of the phenyl group recorded higher shifts in T_{1rho} for both the experiments. But even more interestingly, observing the results on the T_{1rhoC} the carbon corresponding to the peak n°3 (4.17) present the largest shift in relaxation time. This could be due to the fact that the motions reported by the PEA cation, include a phenyl ring flip of 180° and a rotational motion of the ethyl chain in two points. The first is generally a faster movement that the latter [44] Regardless, this means that the C_3 is subjected to two different types of movements of the molecule. This also suggests that the disorder might be caused by fast re-orientations of the cation inside the lattice, which include both the phenyl ring flip and the rotations of the ethyl group. The TORCHIA and T_{1rho} relaxation measurements can be viewed as complementary, as they give information about long to medium range movements of the organic molecule involved. In This case, the two experiments combined, finally proved that the two perovskites' organic layer have a different degree of disorder, and therefore the organic cations of the PEA_1 perovskite present a much higher mobility compared to the PEA_2. These results also clarify the variations in chemical shifts and the resolution of the spectra observed for all the examined nuclei. Since the only distinction between the two compounds is the precursor used in their synthesis, it is likely that this factor accounts for the intriguing differences. As the varying precursors may influence the orientation and, consequently, the disorder of the organic layers during the crystallization of the perovskites.

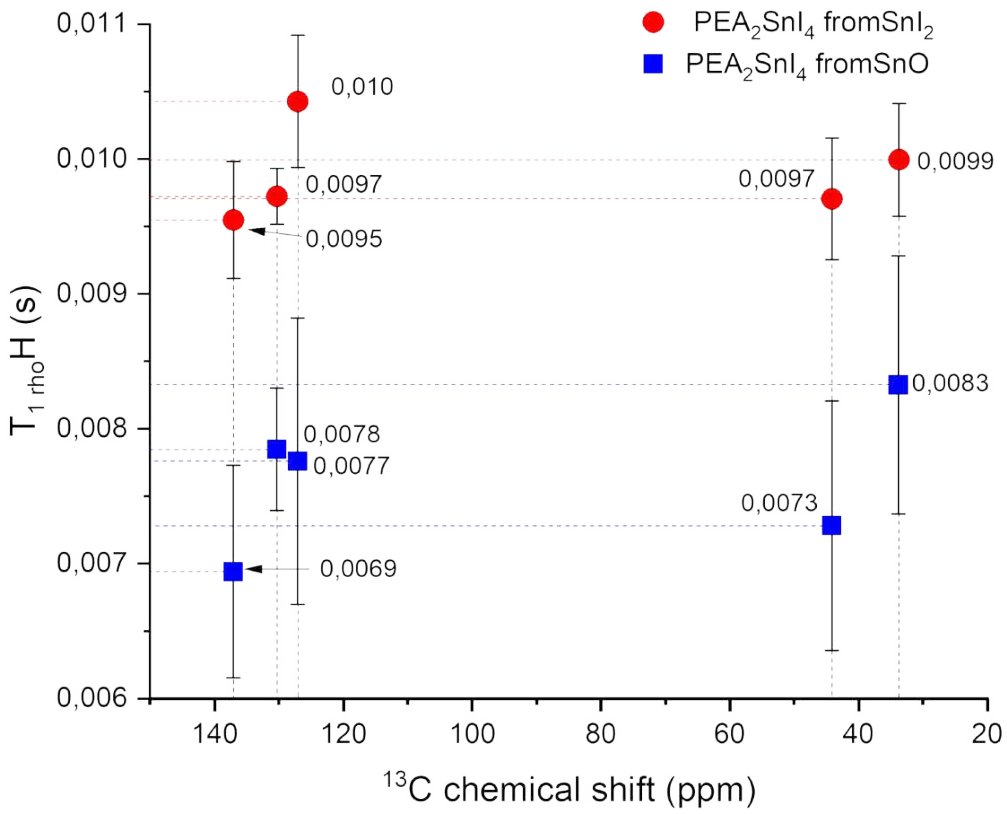

Figure 4.18: spin lattice relaxation in the rotating frame on proton, acquired with MASR=25kHz and T=298K: comparison between PEA_1 and PEA_2

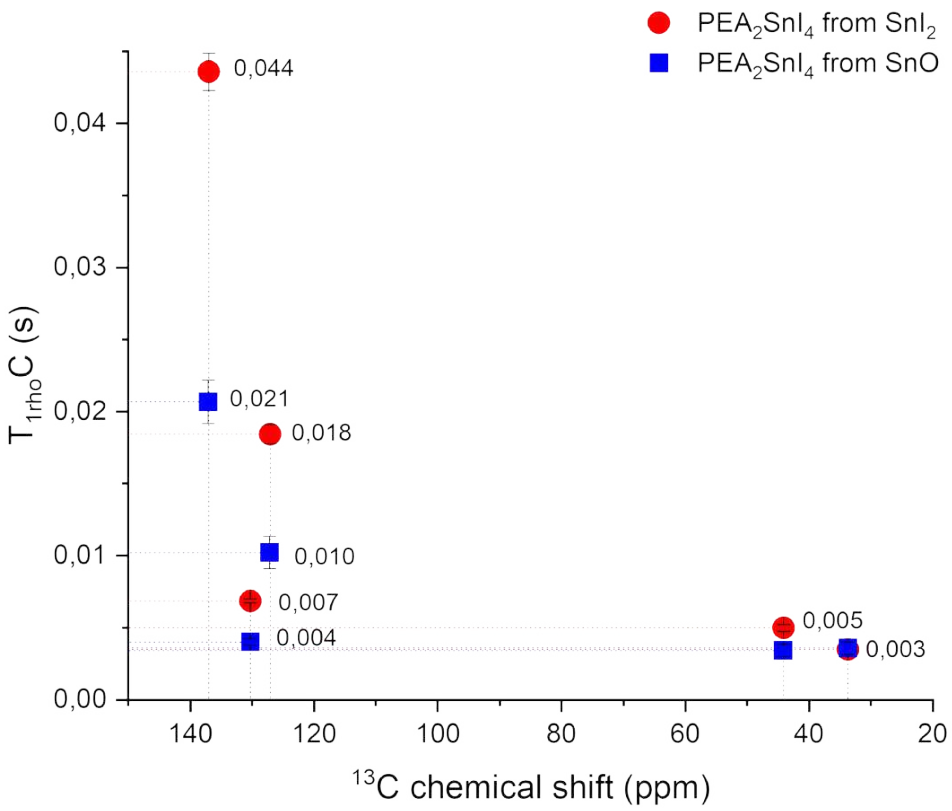

Figure 4.19: spin lattice relaxation in the rotating frame on carbon-13, acquired with MASR=25kHz and T=298K: comparison between PEA_1 and PEA_2

Conclusions and future perspectives

For the purpose of this work, two hybrid perovskites were synthesised: $FASnI_3$ and PEA_2SnI_4 starting form two different precursors, SnO and SnI_2. The aim of the study is the characterization of their structure through a combination of solid state NMR and single crystal XRD. The main focus was on the two samples of PEA_2SnI_4: PEA_1 and PEA_2, as they presented some discrepancies in the ss-NMR spectra and XRD results. The use of both techniques allowed for a comprehensive view of the structure and the dynamics of the perovskites, providing information about the structural disorder of the crystals and the mobility of the atoms. In fact, the two samples were initially characterised by SC-XRD, which provided slightly different results for the two perovskites, suggesting that the degree of disorder in the structure of PEA_1 is higher than the one recorded on PEA_2. Therefore, ss-NMR experiments were performed on ^{1}H, ^{13}C and ^{119}Sn. The most intersting outcomes were provided by the ^{119}Sn spectra. In fact, the results obtained by the $^{1}H/^{119}Sn$ CP, reported two completely different spectra, where the PEA_1 spectrum resulted in flat line, as opposed to PEA_2 where the tin signal was clearly acquired. At the same time, the Hahn echo experiments revealed a shift of $\sim$ 10ppm between each other, and one of $\sim$ 50ppm with the CP. The first shift can be traced to a different local environment on tin, suggesting that the two samples present differences in the organic layer of the perovskite. Similar conclusions can be derived by the shift with CP, since this experiment is highly influenced by the vicinity of the atoms and the mobility of the protons. This indicates that the organic cations in PEA_1 are actually more mobile than the ones on PEA_2, resulting in a higher structural disorder. These results were confirmed by the relaxation measurements carried out on ^{13}C. The two types of relaxation experiments performed include TORCHIA, which reports T_1 on carbon, and spin lattice relaxation on the rotating frame, that is able to fit the T_{1rhoH} and T_{1rhoC}. These two measurements can

be viewed as complementary, as TORCHIA records long range movements of the atoms, corresponding to side chain rotations, while the relaxations in the rotating frame provide information about faster movements, as phenyl ring flips. The results of these experiments remark the differences in the two samples, as the relaxation times of the carbons in PEA_1 are notably shorter than those in PEA_2, particularly concerning the aromatic carbons.
It can be concluded that the two structures exhibit significant differences in the mobility of the organic cations. These variations stem from the use of different precursors during the synthesis of the perovskites. This work also demonstrates that combining solid-state NMR and XRD techniques can be an effective approach for enhancing research on the structure of perovskites, as well as their mobility and dynamics. While further measurements are needed to establish precise correlations between the organic and inorganic layers, and even among the atoms within the PEA cation itself, this study serves as a good foundation for future research in this area. In fact, further studies should be dedicated to the influence that the choice of the precursor can have on the crystal structure of the perovskite, allowing a more thoughtful selection of the materials, which can be crucial for improving the quality and efficiency of perovskites regarding their applications in the photovoltaic and optoelectronic fields.

Bibliography

[1] Kim, J. Y., Lee, J., Jung, H. S., Shin, H., and Park, N. (2020). High-Efficiency Perovskite solar cells. Chemical Reviews, 120(15), 7867–7918. https://doi.org/10.1021/acs.chemrev.0c00107

[2] Rosales, B. A., Hanrahan, M. P., Boote, B. W., Rossini, A. J., Smith, E. A., & Vela, J. (2017). Lead halide perovskites: Challenges and opportunities in advanced synthesis and spectroscopy. ACS Energy Letters, 2(4), 906–914. https://doi.org/10.1021/acsenergylett.6b00674

[3] Mitzi, D., & Liang, K. (1997). Synthesis, resistivity, and thermal properties of the cubic perovskite NH2CH=NH2SNI3and related systems. Journal of Solid State Chemistry, 134(2), 376–381. https://doi.org/10.1006/jssc.1997.7593

[4] Sato, T., Takagi, S., Deledda, S., Hauback, B. C., and Orimo, S. (2016). Extending the applicability of the Goldschmidt tolerance factor to arbitrary ionic compounds. Scientific Reports, 6(1). https://doi.org/10.1038/srep23592

[5] Liu, R., Hu, X., Xu, M., Ren, H., & Yu, H. (2023). Layered Low-Dimensional Ruddlesden-Popper and Dion-Jacobson perovskites: from material properties to photovoltaic device performance. ChemSusChem, 16(19). https://doi.org/10.1002/cssc.202300736

[6] Mao, L., Stoumpos, C. C., & Kanatzidis, M. G. (2018). Two-Dimensional Hybrid Halide Perovskites: Principles and promises. Journal of the American Chemical Society, 141(3), 1171–1190. https://doi.org/10.1021/jacs.8b10851

[7] Cortecchia D. Slides Introduction to metal halide perovskite, lecture. Lecture presented at: Lezione metal halide perovskites; 2024 Apr 10; Università di Bologna

[8] Pelant, I.,& Valenta, J. (2012). Luminescence spectroscopy of semiconductors. In Oxford University Press eBooks. https://doi.org/10.1093/acprof:oso/9780199588336.001.0001

[9] Exciton: An Introduction. (n.d.). Ossila. https://www.ossila.com/pages/what-is-an-exciton

[10] Umebayashi, T., Asai, K., Kondo, T., & Nakao, A. (2003). Electronic structures of lead iodide based low-dimensional crystals. Physical Review. B, Condensed Matter, 67(15). https://doi.org/10.1103/physrevb.67.155405

[11] Wang, K., Park, J. Y., Akriti, N., & Dou, L. (2021). Two-dimensional halide perovskite quantum-well emitters: A critical review. EcoMat, 3(3). https://doi.org/10.1002/eom2.12104

[12] Anta, J. A., Oskam, G., & Pistor, P. (2024). The dual nature of metal halide perovskites. The Journal of Chemical Physics, 160(15). https://doi.org/10.1063/5.0190890

[13] Wang, K., Yang, P., Chen, Y., Kang, Z., Cao, L., Wang, H., Huo, J., Li, T., Tong, Y., & Wang, H. (2023). Rational selection of phenethylammonium salts for 2D/3D tin perovskite solar cells: The halogen ion matters. ACS Applied Energy Materials, 6(20), 10509–10517. https://doi.org/10.1021/acsaem.3c01651

[14] Pitaro, M., Tekelenburg, E. K., Shao, S., & Loi, M. A. (2021). Tin Halide perovskites: from fundamental properties to solar cells. Advanced Materials, 34(1). https://doi.org/10.1002/adma.202105844

[15] Wan, Z., Lai, H., Ren, S., He, R., Jiang, Y., Luo, J., Chen, Q., Hao, X., Wang, Y., Zhang, J., Wu, L., & Zhao, D. (2020). Interfacial engineering in lead-free tin-based perovskite solar cells. Journal of Energy Chemistry, 57, 147–168. https://doi.org/10.1016/j.jechem.2020.08.053

[16] Reif, B., Ashbrook, S. E., Emsley, L., and Hong, M. (2021). Solid-state NMR spectroscopy. Nature Reviews Methods Primers, 1(1). https://doi.org/10.1038/s43586-020-00002-1

[17] Spinelli, A., (2011) Resine epossidiche: studio delle proprietà microscopiche mediante NMR in stato solido, Tesi di dottorato, Università di Padova

[18] Libretexts. (2020, July 14). 12.3: Chemical shifts and shielding. Chemistry LibreTexts.https://chem.libretexts.org/Bookshelves/Organic_Chemistry/Map%3A_Organic_Chemistry_(Wade)_Complete_and_Semesters_I_and_II/Map%3A_Organic_Chemistry_(Wade)/12%3A_Nuclear_Magnetic_Resonance_Spectroscopy/12.03%3A_Chemical_Shifts_and_Shielding

[19] Borsacchi, S., Bonaccorsi, M., Mais, M., Callucci, L., Carignani, E., Martini, F., & Geppi, M. (2017). NMR ALLO STATO SOLIDO: UNA TECNICA FONDAMENTALE PER LO STUDIO DI FARMACI e MATERIALI. Chimica & Materiali, 20–26. https://doi.org/10.17374/CI.2015.97.4.20

[20] Tošner, Z., Brandl, M. J., Blahut, J., Glaser, S. J., & Reif, B. (2021). Maximizing efficiency of dipolar recoupling in solid-state NMR using optimal control sequences. Science Advances, 7(42). https://doi.org/10.1126/sciadv.abj5913

[21] Duer, M. J. Solid-State NMR Spectroscopy Principles and Applications. (2001). In Wiley eBooks. https://doi.org/10.1002/9780470999394

[22] Majumdar, R. D. (2015b). A nuclear magnetic resonance spectroscopic investigation of the molecular structure and aggregation behavior of asphaltenes. https://opus.uleth.ca/handle/10133/4526

[23] Chierotti, M. R., and Gobetto, R. (2012). Solid-State NMR Studies on Supramolecular Chemistry. John Wiley & Sons, Ltd.https://doi.org/10.1002/9780470661345.smc026

[24] Piveteau, L., Morad, V., & Kovalenko, M. V. (2020). Solid-State NMR and NQR spectroscopy of Lead-Halide perovskite materials. Journal of the American Chemical Society, 142(46), 19413–19437. https://doi.org/10.1021/jacs.0c07338

[25] Franssen, W. M., & Kentgens, A. P. (2019). Solid–state NMR of hybrid halide perovskites. Solid State Nuclear Magnetic Resonance, 100, 36–44. https://doi.org/10.1016/j.ssnmr.2019.03.005

[26] Hope, M. A., Nakamura, T., Ahlawat, P., Mishra, A., Cordova, M., Jahanbakhshi, F., Mladenović, M., Runjhun, R., Merten, L., Hinderhofer, A., Carlsen, B. I., Kubicki, D. J., Gershoni-Poranne, R., Schneeberger, T., Carbone, L. C., Liu, Y., Zakeeruddin, S. M., Lewinski, J., Hagfeldt, A., . . . Emsley, L. (2021). Nanoscale Phase Segregation in Supramolecular π-Templating for Hybrid Perovskite Photovoltaics from NMR Crystallography. Journal of the American Chemical Society, 143(3), 1529–1538. https://doi.org/10.1021/jacs.0c11563

[27] Kubicki, D. J., Prochowicz, D., Hofstetter, A., Péchy, P., Zakeeruddin, S. M., Grätzel, M., & Emsley, L. (2017). Cation Dynamics in Mixed-Cation (MA)x(FA)1–xPbI3 Hybrid Perovskites from Solid-State NMR. Journal of the American Chemical Society, 139(29), 10055–10061. https://doi.org/10.1021/jacs.7b04930

[28] Kubicki, D. J., Prochowicz, D., Salager, E., Rakhmatullin, A., Grey, C. P., Emsley, L., & Stranks, S. D. (2020). Local Structure and Dynamics in Methylammonium, Formamidinium, and Cesium Tin(II) Mixed-Halide Perovskites from 119Sn Solid-State NMR. Journal of the American Chemical Society, 142(17), 7813–7826. https://doi.org/10.1021/jacs.0c00647

[29] Ueda, T., Shimizu, K., Ohki, H., & Okuda, T. (1998). 13CP/MAS NMR Study of Motion and Local Structure of Phenethyl- ammonium Ion in [C6H5CH2CH2 NH3]2PbX4(X = Cl, Br, I). Zeitschrift Für Naturforschung A, 53(12), 983–988. https://doi.org/10.1515/zna-1998-1209

[30] Alvarado-Leaños, A. L., Cortecchia, D., Saggau, C. N., Martani, S., Folpini, G., Feltri, E., Albaqami, M. D., Ma, L., & Petrozza, A. (2022). Lasing in Two-Dimensional tin perovskites. ACS Nano, 16(12), 20671–20679. https://doi.org/10.1021/acsnano.2c07705

[31] Femoni C. Slides: X-Ray Diffraction, lecture. Università di Bologna

[32] Bunaciu, A. A., Udriştioiu, E. G., & Aboul-Enein, H. Y. (2015). X-Ray diffraction: instrumentation and applications. Critical Reviews in Analytical Chemistry, 45(4), 289–299. https://doi.org/10.1080/10408347.2014.949616

[33] Princeton Instruments. (2021, September 21). Introduction to X-ray scattering. Teledyne Princeton Instruments. https://www.princetoninstruments.com/learn/x-ray-scattering/introduction-to-x-ray-diffraction

[34] Kahmann, S., Nazarenko, O., Shao, S., Hordiichuk, O., Kepenekian, M., Even, J., Kovalenko, M. V., Blake, G. R., and Loi, M. A. (2020). Negative thermal quenching in FASNI3 perovskite single crystals and thin films. ACS Energy Letters, 5(8), 2512–2519. https://doi.org/10.1021/acsenergylett.0c01166

[35] University of Boston, (2021) Basic NMR Concepts: A Guide for the Modern Laboratory https://www2.chemistry.msu.edu/courses/cem845/FS21/DH%20NMR%20Basics_17.pdf

[36] Texas A & M University (2022) NMR Parameter Primer https://nmr.tamu.edu/pdf/tidbits/NMRTotM_202203.pdf

[37] J. Struppe, S. Steuernagel, F. Aussenacc, F. Benevelli, P. Gierth, & S. (2016) Wegner Solid State NMR; AVANCE Solids User Manual (Version 003). Brucker Corporation.

[38] Apperley, D.C., Harris, R.K. & Hodgkinson p. (2012) Solid-State NMR: basic principles & practice. Momentum Press, LLC.

[39] Müller, K., & Geppi, M. (2021). Solid State NMR: Principles, Methods, and Applications. John Wiley & Sons

[40] Pascual, J., Di Girolamo, D., Flatken, M. A., Aldamasy, M. H., Li, G., Li, M., & Abate, A. (2021). Lights and shadows of DMSO as solvent for tin halide perovskites. Chemistry - a European Journal, 28(12). https://doi.org/10.1002/chem.202103919

[41] Finkenauer, B. P., Akriti, N., Ma, K., & Dou, L. (2022). Degradation and Self-Healing in perovskite solar cells. ACS Applied Materials & Interfaces, 14(21), 24073–24088. https://doi.org/10.1021/acsami.2c01925

[42] Zhang, T., Zhou, C., Feng, X., Dong, N., Chen, H., Chen, X., Zhang, L., Lin, J., & Wang, J. (2022). Regulation of the luminescence mechanism of two-dimensional tin halide perovskites. Nature Communications, 13(1). https://doi.org/10.1038/s41467-021-27663-0

[43] Folpini, G., Palummo, M., Cortecchia, D., Moretti, L., Cerullo, G., Petrozza, A., Giorgi, G., & Kandada, A. R. S. (2023). Plurality of excitons in Ruddlesden–Popper metal halides and the role of the B-site metal cation. Materials Advances, 4(7), 1720–1730. https://doi.org/10.1039/d2ma00136e

[44] Ueda, T., Omo, M., Shimizu, K., Ohki, H., & Okuda, T. (1997). Ionic motion of phenethylammonium ion in [C6H5CH2CH2NH3]2 PBX4 (X = CL, BR, I) as studied by 1 h NMR. Zeitschrift Für Naturforschung A, 52(6–7), 502–508. https://doi.org/10.1515/zna-1997-6-706